



Cite this: *Dalton Trans.*, 2016, **45**, 7678

Chemical state determination of molecular gallium compounds using XPS†

Jeremy L. Bourque,^a Mark C. Biesinger^b and Kim M. Baines*^a

A series of molecular gallium compounds were analyzed using X-ray photoelectron spectroscopy (XPS). Specifically, the Ga 2p_{3/2} and Ga 3d_{5/2} photoelectron binding energies and the Ga L₃M₄₅M₄₅ Auger electron kinetic energies of compounds with gallium in a range of assigned oxidation numbers and with different stabilizing ligands were measured. Auger parameters were calculated and used to generate multiple chemical speciation (or Wagner) plots that were subsequently used to characterize the novel gallium–cryptand[2.2.2] complexes **1–3** that possess ambiguous oxidation numbers for gallium. The results presented demonstrate the ability of widely accessible XPS instruments to experimentally determine the chemical state of gallium centers and, as a consequence, provide deeper insights into reactivity compared to assigned oxidation and valence numbers.

Received 26th February 2016,
Accepted 30th March 2016

DOI: 10.1039/c6dt00771f

www.rsc.org/dalton

Introduction

The chemical state of the key atoms in novel inorganic complexes is a vital piece of information for understanding reactivity. Two formalisms exist for classifying the atoms of interest in a new compound: oxidation or valence numbers.¹ As put forth by Parkin, the oxidation number can be described as “...the charge remaining on an atom when all ligands are removed heterolytically...”, with the electron pairs involved in bonding given to the atom with the larger electronegativity. Conversely, valence indicates the “number of electrons that an atom uses in bonding”.² While the oxidation and valence numbers are sometimes equal, many examples exist for main group compounds where this is not the case. As an example, Group 13 halides in their monomeric forms are assigned an oxidation and valence number of +3, illustrated using BF₃ in Fig. 1. In B₂F₄, each boron atom is assigned an oxidation number of +2, and a valence number of 3.² Both compounds react primarily as Lewis acids, despite their different oxidation numbers,^{3,4} and demonstrate that one measure alone cannot be used to predict the reactivity of main group compounds.

Although Parkin argues that the valence number of an atom is more reflective of its chemical state, several main group complexes do not follow this narrative. For example, in Scheme 1, although both compounds have valence numbers of

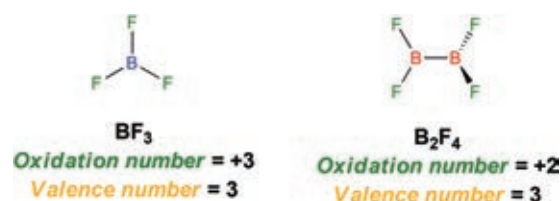
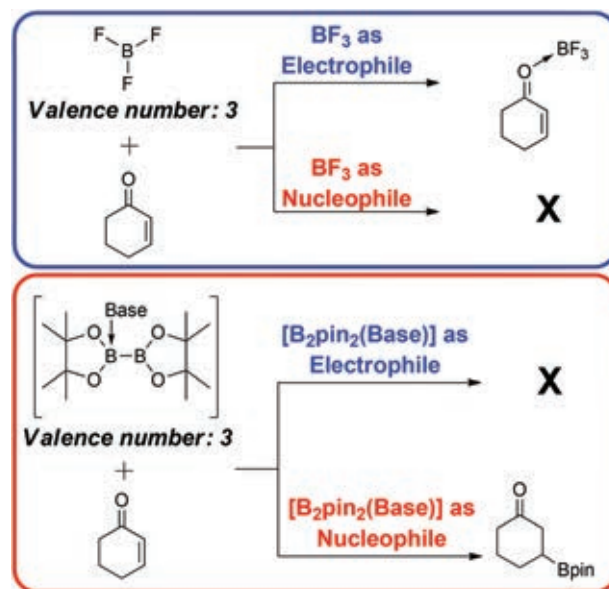


Fig. 1 Differences in oxidation and valence numbers for BF₃ and B₂F₄.



Scheme 1 Example of how the valence number can fail to accurately predict reactivity.

^aDepartment of Chemistry, University of Western Ontario, London, Ontario, Canada, N6A 5B7. E-mail: kbaines2@uwo.ca

^bSurface Science Western, University of Western Ontario, London, Ontario, Canada, N6G 0J3

† Electronic supplementary information (ESI) available. See DOI: 10.1039/c6dt00771f

3, BF_3 reacts as a Lewis acid and an electrophile, coordinating to the oxygen atom of 1-cyclohex-2-enone.⁵ Conversely, if a base such as a phosphine or methoxide is added to B_2pin_2 (pin = pinacolato), the boron fragment acts as a nucleophile, resulting in addition to the alkene, demonstrating that the construct of valence numbers can fail when attempting to predict reactivity.⁶

Another example where valence numbers do not properly predict reactivity is observed for unsaturated main group compounds, examples of which are shown in Fig. 2. Here, a multiply bonded digallene⁷ and disilene⁸ are shown, along with their assigned oxidation and valence numbers. While the valence numbers depict main group centers that are using all of their available electrons for bonding, their oxidation numbers demonstrate that these two complexes are reactive toward a variety of organic and inorganic substrates.^{9,10} It is evident that while chemically intuitive qualitative descriptors can aid in the prediction of reactivity, experimentally determined measures of the chemical state of a given atom in a compound are needed.

As with its lighter congeners, gallium chemistry has many examples where the assigned oxidation number and reactivity of a given complex may not correlate. Often, the oxidation numbers of individual atoms may not be immediately evident upon initial scrutiny, and depending on the compound, the formalism of oxidation numbers may not accurately represent the reactivity of the molecule. It is, therefore, important to use a measure that has an experimental basis that can correctly give indications as to what types of reactivity can be expected. As examples, the structural and bonding characteristics of two common “low valent” gallium starting materials, ‘GaI’ and Ga_2Cl_4 , have required extensive studies to firmly establish the compositions of both compounds and to understand their reactivity.

As the crystal structure of ‘GaI’ could not be determined due to its insolubility, susceptibility to disproportionation in donor solvents, variable composition, and amorphous nature, only spectroscopic and diffraction methods have been used to determine the composition of ‘GaI’.¹¹ A recent study utilizing Raman, ^{71}Ga solid-state NMR, and ^{127}I NQR spectroscopies and powder X-ray diffraction has revealed that, depending on

the reaction time, ‘GaI’ can have vastly different compositions; its chemical formula was found to be either $[\text{Ga}^0]_2[\text{Ga}^+][\text{GaI}_4^-]$ or $[\text{Ga}^0]_2[\text{Ga}^+][\text{Ga}_2\text{I}_6^{2-}]$.¹¹ The formulae were elucidated using the chemical shift values and quadrupolar coupling constants of the ^{71}Ga solid-state NMR signals, and the unique frequencies of the ^{127}I NQR signals of the multiple iodide environments present in the ‘GaI’ samples. Despite its variable composition and the presence of higher oxidation numbers within the sample, the reactivity of ‘GaI’ can mostly be attributed to the gallium(I) centers, but the occurrence of gallium(II) and gallium(III) products can be attributed to the ease with which Lewis bases can cause disproportionation of the gallium(I) cation or the existence of gallium centers with higher oxidation numbers in the starting material.

Similarly, the structure of Ga_2Cl_4 was initially unknown, and it was uncertain as to whether Ga_2Cl_4 was a gallium(II) compound containing a gallium–gallium bond with equivalent gallium centers, or a mixed valent salt with a gallium(I) cation and a tetrachlorogallate(III) anion (Fig. 3). Following successful crystallization, it was determined that the latter description was the most accurate.¹² As an added complexity, comproportionation of Ga_2Cl_4 from $[\text{Ga}][\text{GaCl}_4]$ to $\text{Cl}_2\text{GaGaCl}_2$ readily occurs upon the addition of a Lewis base to the complex.¹³ ^{35}Cl and $^{69/71}\text{Ga}$ solid-state NMR spectroscopy have also been utilized to characterize $[\text{Ga}][\text{GaCl}_4]$. Two gallium environments exist: the gallium(I) signal is centered around -610 ppm, and the tetrachlorogallate(III) signal is located at 231 ppm.^{14,15} While the significant difference in the electronic nature between the two sites allows for easy characterization and assignment in this salt, in more complex species, it may be more difficult to assign an oxidation number based on chemical shifts or quadrupolar coupling constants.

Examples where the oxidation number of gallium in a given complex is ambiguous despite knowing the molecular structure often arise when multiple atoms of a given element are bound together, or when a gallium center is bound by ligands that are capable of hosting electron delocalization or a negative charge. An example is shown in Fig. 4. Here, a $[\text{Ga}_5\text{I}_4]^{3+}$ fragment stabilized by NacNac ligands can be described by multiple bonding descriptors, two of which are shown. The ambiguity of the bonding in this compound cannot be resolved through structural or traditional spectroscopic

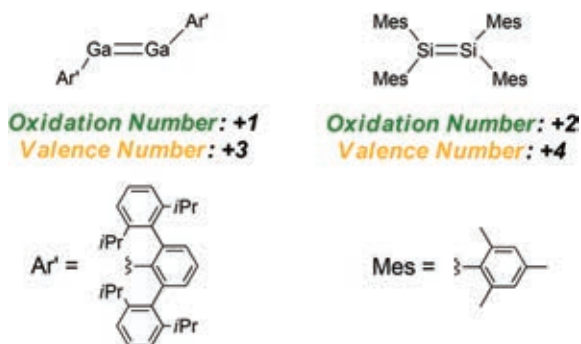


Fig. 2 Oxidation and valence numbers of a digallene and a disilene.

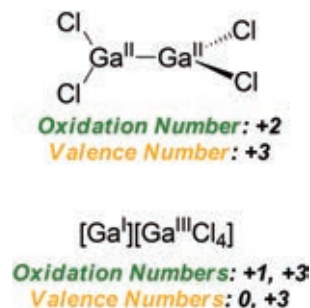


Fig. 3 Two possible structures of Ga_2Cl_4 .

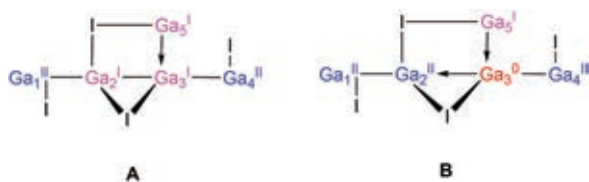


Fig. 4 Two bonding models for the $[\text{Ga}_5\text{I}_4]^{3+}$ core of $[\text{Ga}_5\text{I}_4(\text{t}^{\text{Bu}}\text{MesNacNac})_3]$, with the NacNac ligands removed for clarity.

methods typically employed by synthetic chemists, highlighting the need for alternative techniques for chemical state determination.¹⁶

We have recently reported the synthesis of novel cationic multinuclear gallium–cryptand[2.2.2] complexes, **1** and **2**. Despite extensive characterization using the standard spectroscopic techniques and analysis of the bonding using computational methods, the oxidation numbers of the gallium centers were ambiguous.¹⁷ Thus, we sought out a means to assess the chemical state of the gallium in these complexes to aid in the prediction and rationalization of their reactivity.

Experimental techniques for chemical state elucidation

Very few analytical methods for the evaluation of the chemical states of main group elements exist. One well-known technique is Mössbauer spectroscopy. This method uses γ -irradiation to induce a nuclear transition in the sample. Although Mössbauer spectroscopy is extremely sensitive and is very effective at distinguishing chemical states of certain elements, the technique is somewhat limited since few elements of the periodic table have adequate γ -ray sources and γ -ray sources are subject to decay.^{18,19} Although Mössbauer spectroscopy has been used for many years as an effective technique to probe the bonding and chemical states of molecular tin and iron compounds,^{20–22} more widely accessible techniques for chemical state determination are desired for those elements which do not possess a suitable Mössbauer source.

Another spectroscopic method that has been utilized for the assessment of the chemical state of main group compounds is solid-state NMR spectroscopy. Our group has used ³⁵Cl solid-state NMR spectroscopy as an indirect probe for evaluating the chemical state of a range of chlorogermanes. The magnitude of the quadrupolar coupling constant (C_Q) of the ³⁵Cl signal was found to correlate to the oxidation number of the germanium center.²³ While this has been shown to be effective, methods which probe the element of interest directly and are more generally applicable are desired.

X-ray absorption near edge structures (XANES) has been commonly employed to evaluate the local geometry and chemical state of a given atom in a molecular compound or material.^{24–26} There are, however, many disadvantages to using XANES to probe the chemical state of a given element; a syn-

chrotron is required to perform such experiments, and significant expertise in this field is required for data acquisition and interpretation limiting the use of XANES. Nonetheless, XANES has much promise in this endeavor.²⁷

Another technique that has been used for chemical state elucidation is X-ray photoelectron spectroscopy (XPS). Unlike the aforementioned ³⁵Cl solid-state NMR spectroscopic study for germanium compounds, the presence of an indirect probe, in this case a chloride ligand, is not required, as the data obtained pertains directly to the element being examined. Similar to XANES, XPS provides information on the chemical state of the atom using X-ray radiation. Unlike XANES, the technique is widely accessible, as a synchrotron is not required. XPS can be used to analyze most solid samples and can detect all elements except for hydrogen and helium. Although XPS has been utilized primarily for surface analysis and speciation, it may be applied to molecular compounds as well, despite the rarity of such reports in the literature. The dearth of XPS studies on molecular compounds may arise from the potential for surface contamination, as often contaminants remain in the analysis chamber, which, despite the ultra-high vacuum, may deposit on the surface of the sample. In some cases, when the contaminant contains the primary element of focus for a particular study, the data obtained may be affected. However, this is not the case for many main group elements, as they are rarely observed as contaminants. While contamination of the sample may result in a decrease in the desired signal intensity, this is not a significant problem if the signal of interest is of a sufficient strength.²⁸

The initial process of performing XPS is straightforward. A sample is placed inside an observation chamber that has been put under ultra-high vacuum ($\sim 10^{-9}$ Torr). The sample, which is spread onto a sample holder, forming a surface, is bombarded by high-energy X-ray photons (E_{hv}) (typically monochromatic Al K(α) radiation at 1486.71 eV or Mg K(α) at 1253.6 eV). This causes the expulsion of core electrons from the atoms present in the sample, termed photoelectron emission. The kinetic energy of the photoelectrons is measured, and is related to the binding energy of the electrons by eqn (1):

$$E_{\text{K}} = E_{\text{hv}} - E_{\text{B}} - \phi_{\text{XPS}} \quad (1)$$

where E_{K} is the kinetic energy of the photoelectron, ϕ_{XPS} is the work function of the XPS spectrometer, and E_{B} is the binding energy of the photoelectron. The binding energy is specific to each orbital for each element of the periodic table. The usefulness of XPS relies on the fact that the binding energies shift depending on the chemical state of the atom. The chemical state can be thought of as any variable that can affect the nature of the atom being observed. For example, changes in oxidation or valence number, ligand type, and charge can affect the chemical state of an atom and the binding energies of its photoelectrons. While using only binding energies to probe the chemical state of certain elements can be somewhat

inaccurate, the use of the Auger parameter can improve the accuracy of these measurements.²⁸

The original definition of the Auger parameter is shown in eqn (2):

$$\alpha = E_{\text{k}}(\text{Auger}) - E_{\text{k}} \quad (2)$$

$$\alpha' = E_{\text{B}} + E_{\text{k}}(\text{Auger}) \quad (3)$$

where E_{k} is the kinetic energy of the photoelectron, and $E_{\text{k}}(\text{Auger})$ is the kinetic energy of the Auger electron.²⁹ Auger electron emission results from a relaxation mechanism, whereby an atom, which has emitted a photoelectron, fills its core hole, resulting in the simultaneous emission of an Auger electron from a higher orbital, and the repopulation of the core hole by an electron from the same orbital. The Auger electron kinetic energy is dependent on the valence electron richness of the atom being analyzed: as the electron richness increases, the kinetic energy also increases. Although the original Auger parameter was defined as the difference of the kinetic energies of the photo- and Auger electrons, the modified Auger parameter (eqn (3)), which is the sum of the photoelectron binding energy and the Auger electron kinetic energy, is independent of the X-ray energy used. The reasoning behind using the Auger parameter in determining differences in chemical states arises from the stronger influence of the environment of the atom on the Auger electron energies for some elements, as well as combining the influence of both the photo- and Auger electron energies. This is an important consideration for insulators and semi-conductors, as the accumulation of charge on the sample can result in significant deviations in electron energies. Additionally, any surface charging shifts will be of the same magnitude, but of the opposite direction in each of the components, and any associated error will be eliminated.³⁰ The modified Auger parameter has been extensively studied and utilized, and therefore, is now the accepted definition.³¹ Several reviews have been published in recent years, outlining the mathematical and theoretical background to using the Auger parameter for the differentiation of chemical states.^{30,32}

The Auger parameter has been used for many elements of the periodic table and its effectiveness is maximized when the data are presented in a graphical plot. These are known as chemical speciation or Wagner plots. An example is shown in Fig. 5. Wagner plots contain three axes: on the left axis, the Auger electron kinetic energy ($E_{\text{k}}(\text{Auger})$, or $E_{\text{k}}(\text{C}'\text{C}''\text{C}''')$); these are expressed in X-ray notation, *i.e.* LMM²⁸); on the bottom, the photoelectron binding energy (E_{B} , or $E_{\text{B}}(\text{C})$); this is presented in spectroscopic notation, *i.e.* 2p_{3/2}); and on the right axis, the modified Auger parameter (α). The definition of the Auger parameter leads to the generation of lines with a slope of 1, which are equal to the value of the Auger parameter, with the intercepts being equal to the photoelectron binding energy and the Auger electron kinetic energy for the x and y axes, respectively. Wagner plots are known to be effective in chemical state determination, allowing the differences in photoelectron binding energy and

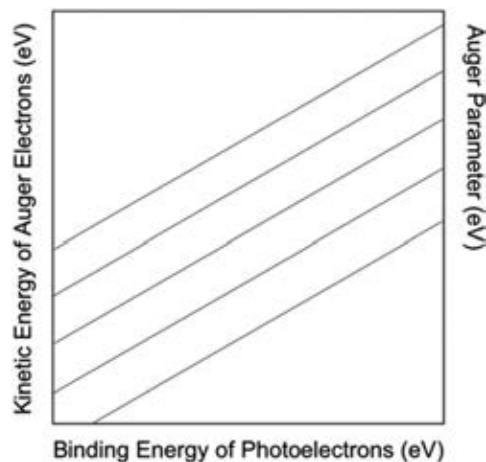


Fig. 5 A generic Wagner plot.

the Auger electron kinetic energy to be visualized. Although the use of the Auger parameter and Wagner plots aids in the determination of chemical states, the Auger parameter itself is not a measure of the electron deficiency or richness of a given element, as compounds with vastly different electronic environments may have similar Auger parameter values.

An additional aspect of chemical state differentiation that can be extracted from the Auger parameter and Wagner plots are whether the differences between compounds are more strongly influenced by initial or final state effects. Initial state effects are shifts in the orbital energies of an atom before it is subject to X-ray radiation. These effects are highly dependent on the nature of the ligands bound to the element of interest. In essence, the partial charge induced at the atom by the attached ligands gives rise to significant deviations in the binding energy observed. These deviations can be thought of as a type of chemical shift. An example is the change in binding energy as halide ligands are varied down Group 17, as the binding energy is expected to decrease due to increased electron density at the central atom. Final state effects result from differences in polarization within the electron cloud of the atom after it has been ionized by X-ray irradiation. Final state effects are often dominant when dealing with compounds that have the potential for significant polarization or electron motility.^{33,34} From Wagner plots, a series of compounds that follow a straight line with a slope equal to 1, meaning they have similar Auger parameter values, have similar final state characteristics, whereas samples that follow a line with a slope of 3, have similar initial state effects.^{30,33} These trends, in some cases, can help discern between differing chemical states of a given element. As an example, when two lines, one with a slope of 1 and one with a slope of 3, are plotted on a Wagner plot for copper compounds and intersect at the data point for copper metal, compounds with a +2 oxidation number generally follow the line with a slope of 3, whereas those with a +1 oxidation number are closer to the line with a slope of 1. These results would indicate that copper

compounds with a +2 oxidation number have similar initial state effects but different final state effects. Alternatively, copper compounds with a +1 oxidation number have similar final state effects but different initial state effects.³³

Although many elements of the periodic table have been extensively studied using XPS and chemical speciation plots, few studies have involved gallium. Although the binding energies of several molecular gallium(III) compounds have been reported,³⁵ most studies have utilized XPS to characterize surfaces and study reactivity and structural features of gallium-containing materials.^{36–44} Only one example of a Wagner plot for gallium compounds has been reported in the literature,³² and while more data exist for other main group elements, these studies generally focus on the characterization of materials and minerals.^{32,45,46} It is therefore of interest to not only demonstrate the applicability of XPS and Wagner plots to elucidate the chemical state of a variety of gallium compounds, but to apply this technique to molecular compounds of other heavier p-block elements. The goal of this study is to analyze a range of standard gallium compounds with a variety of assigned oxidation numbers, electronic and bonding environments using XPS, and to generate Wagner plots to determine the chemical states of these compounds. Distinctions between the assigned oxidation numbers of the known complexes and the experimental chemical states will be made in examples where these quantities differ. Subsequently, three gallium–cryptand[2.2.2] complexes (**1–3**) will be studied by XPS and following the determination of their chemical states, reactivities will be predicted.

Results and discussion

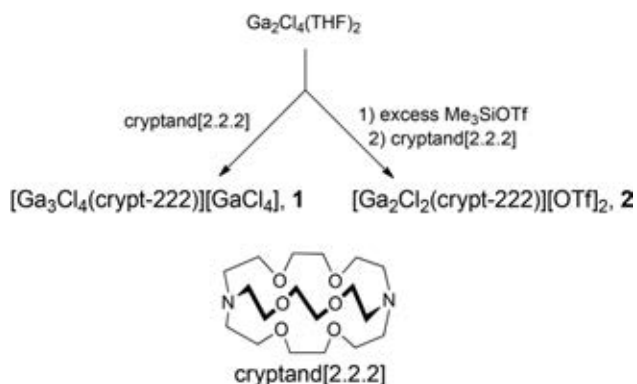
As described previously,¹⁷ several low valent gallium–cryptand [2.2.2] complexes were synthesized from the mixed valent halide salt Ga_2Cl_4 ($[\text{Ga}][\text{GaCl}_4]$).¹² The facile comproportionation of $[\text{Ga}][\text{GaCl}_4]$ was utilized, giving $\text{Ga}_2\text{Cl}_4(\text{THF})_2$,¹³ which was then added to cryptand[2.2.2], both without and in the presence of trimethylsilyl triflate (TMSOTf), leading to the generation of $[\text{Ga}_3\text{Cl}_4(\text{crypt-222})][\text{GaCl}_4]$, **1** and $[\text{Ga}_2\text{Cl}_2(\text{crypt-222})][\text{OTf}]_2$, **2**, respectively (Scheme 2). The

analogous derivative with iodide ligands, $[\text{Ga}_2\text{I}_2(\text{crypt-222})][\text{GaI}_4]_{1.75}[\text{OTf}]_{0.25}$, (**3**), was synthesized from Ga_2I_4 , TMSOTf and cryptand[2.2.2]. Simple bonding descriptors of $[\text{Ga}_3\text{Cl}_4(\text{crypt-222})][\text{GaCl}_4]$ and $[\text{Ga}_2\text{Cl}_2(\text{crypt-222})][\text{OTf}]_2$ could not be unambiguously determined using conventional experimental techniques and computational methods, making it difficult to predict the reactivity of these novel complexes.¹⁷

To understand the chemical states of the gallium centers in complexes **1–3**, a series of gallium compounds with various oxidation numbers and structures were studied using XPS. The compounds are shown in Table 1. A wide range of ligands were chosen to gain as much information as possible on how the binding energies of gallium complexes vary as a function of the ligand, and their influence on the chemical state of the gallium centers. For $\text{Ga}_{(\text{m})}$,^{47–49} GaN,³⁸ GaP,³⁷ GaAs,³⁶ Ga_2O_3 ,^{36,47} and Ga_2Se_3 ,³⁹ XPS data were available from the literature, although experimental data were recollected for $\text{Ga}_{(\text{m})}$ and Ga_2O_3 .^{50,51}

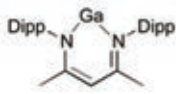
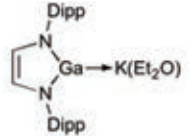
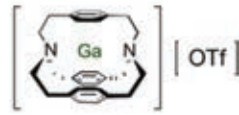
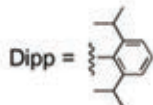
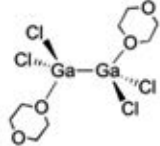
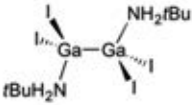
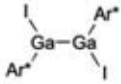

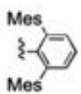
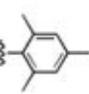
Data collection began with survey scans of each sample. The purity of all synthesized compounds was initially evaluated by multinuclear NMR spectroscopy and ESI-MS before XPS data were collected, nonetheless, some contaminants were observed in the survey spectra. In each spectrum, adventitious carbon was present (C 1s), which was used as an internal charge correction standard set at 284.8 eV. Additionally, the adhesive tape used for sample preparation was carbon-based, leading to a large increase in the atomic percentage of carbon for all samples and skewing the percentages for the other elements present. Other contaminants were oxygen, possibly arising from residual solvent molecules from synthesis of the samples, and fluorine, postulated to arise from leaching of the fluoropolymer from the vial caps used during synthesis and sample transport. The atomic percentages of each element based on the intensities of each signal in the survey spectra can be found in the ESI (Table S1†).

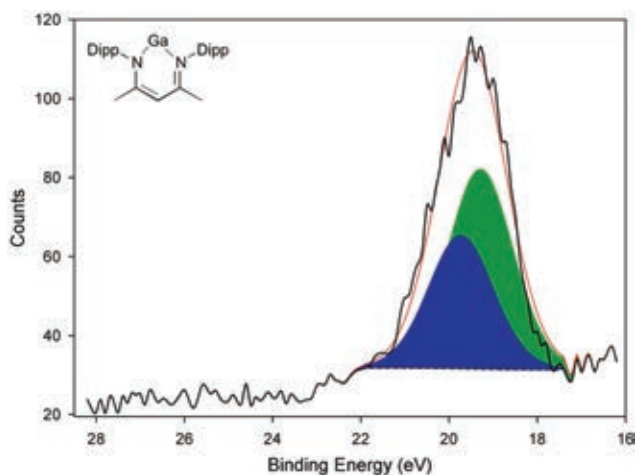
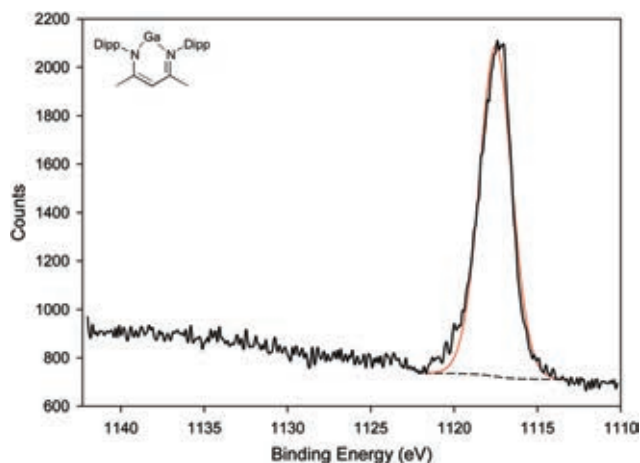
High-resolution XPS spectra were then obtained of each compound. Although two gallium photoelectron signals were observed, namely the Ga 3d and the Ga 2p emissions, the discussion of the results will focus primarily on the Ga 3d photoelectron energies, as it is more intense, and closer in energy to the valence shell of gallium (4p), and thus, more sensitive to subtle changes in the chemical state of gallium. An example of a high-resolution Ga 3d spectrum is shown in Fig. 6 and this spectrum will be used to explain the data analysis process. Initially, one signal is observed, which must be deconvoluted, as the Ga 3d peak is composed of two separate signals at slightly different energies: Ga 3d_{3/2} and Ga 3d_{5/2}. The energy separation is a consequence of spin–orbit splitting, which arises from the difference in the orientation of the emitted photoelectron with respect to the nuclear magnetic field ($m_s = +1/2$ or $-1/2$). These signals were fit with a spin orbit splitting of 0.449 eV, equivalent full-width at half-maxima (FWHM), and a 3d_{5/2} : 3d_{3/2} area ratio of 3 : 2. The fit of these two signals to the experimentally observed spectrum is shown by the red curve. A standard Shirley background was used for all spectral fitting and is shown by the dashed line. The binding energy



Scheme 2 Synthesis of gallium–cryptand[2.2.2] complexes, **1** and **2**.

Table 1 Gallium compounds studied by XPS. Valence numbers are given in parentheses following the compound names

Assigned oxidation number	Compounds			
0	Ga _(metal)			
+1	<div style="display: flex; justify-content: space-around; align-items: flex-start;"> <div style="text-align: center;">  <p>GaNacNac^{Dipp} (1) 4</p> </div> <div style="text-align: center;">  <p>K[GaDAB^{Dipp}] (3) 5</p> </div> <div style="text-align: center;">  <p>[Ga(prismand)][OTf] (0) 6</p> </div> </div> <div style="text-align: center; margin-top: 10px;">  <p>Dipp =</p> </div>			
+2	<div style="display: flex; justify-content: space-around; align-items: flex-start;"> <div style="text-align: center;">  <p>Ga₂Cl₄(diox)₂ (3) 7</p> </div> <div style="text-align: center;">  <p>Ga₂I₄(NH₂tBu)₂ (3) 8</p> </div> <div style="text-align: center;">  <p>Ga₂I₂Ar*₂ (3) 9</p> </div> </div> <div style="text-align: center; margin-top: 10px;">  <p>Ar* =  Mes = </p> </div>			
+3	<table style="width: 100%; border: none;"> <tr> <td style="width: 33%; vertical-align: top;"> GaCl₃ 10 (3) GaCl₂Mes 13 (3) </td> <td style="width: 33%; vertical-align: top;"> GaBr₃ 11 (3) Ga₂Cl₄ 14 (0, 3) </td> <td style="width: 33%; vertical-align: top;"> GaI₃ 12 (3) Ga₂I₄ 15 (0, 3) </td> </tr> </table>	GaCl ₃ 10 (3) GaCl ₂ Mes 13 (3)	GaBr ₃ 11 (3) Ga ₂ Cl ₄ 14 (0, 3)	GaI ₃ 12 (3) Ga ₂ I ₄ 15 (0, 3)
GaCl ₃ 10 (3) GaCl ₂ Mes 13 (3)	GaBr ₃ 11 (3) Ga ₂ Cl ₄ 14 (0, 3)	GaI ₃ 12 (3) Ga ₂ I ₄ 15 (0, 3)		
Ga materials	<table style="width: 100%; border: none;"> <tr> <td style="width: 33%; vertical-align: top;"> GaN 16 (3) Ga₂O₃ 19 (3) </td> <td style="width: 33%; vertical-align: top;"> GaP 17 (3) Ga₂Se₃ 20 (3) </td> <td style="width: 33%; vertical-align: top;"> GaAs 18 (3) </td> </tr> </table>	GaN 16 (3) Ga ₂ O ₃ 19 (3)	GaP 17 (3) Ga ₂ Se ₃ 20 (3)	GaAs 18 (3)
GaN 16 (3) Ga ₂ O ₃ 19 (3)	GaP 17 (3) Ga ₂ Se ₃ 20 (3)	GaAs 18 (3)		

**Fig. 6** Ga 3d signal for GaNacNac^{Dipp}. The experimental (black), simulated (red), component Ga 3d_{3/2} (blue) and Ga 3d_{5/2} (green) and background spectra (dashes) are shown.**Fig. 7** Ga 2p_{3/2} signal for GaNacNac^{Dipp}. The experimental (black), simulated Ga 2p_{3/2} (red) and background spectra (dashes) are shown.

listed for all measurements is that of the Ga $3d_{5/2}$ signals, and not the observed signal maxima. A similar analysis was applied to the Ga $2p_{3/2}$ and Ga $L_3M_{45}M_{45}$ signals (Fig. 7 and 8), however, deconvolution was not necessary for the Ga $2p_{3/2}$ emission, as the Ga $2p_{1/2}$ and the Ga $2p_{3/2}$ signals are completely resolved (1143.2 eV *versus* 1116.4 eV, respectively).²⁸

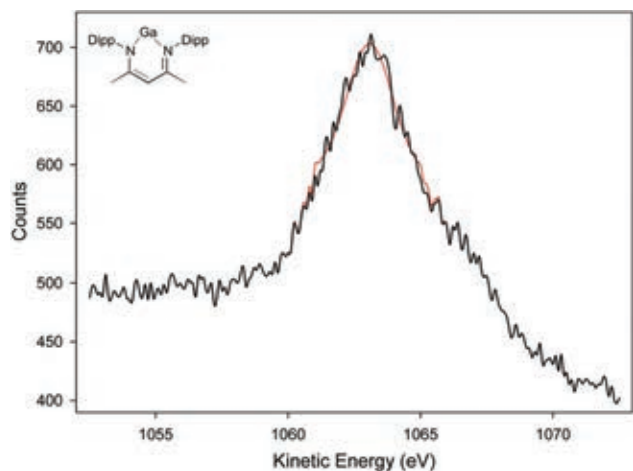


Fig. 8 Ga $L_3M_{45}M_{45}$ signal for GaNacNac^{Dipp}. The experimental (black) and simulated Ga $L_3M_{45}M_{45}$ (red) spectra are shown.

Analysis of the data of the gallium trihalides, GaCl₃, GaBr₃, and GaI₃ (Fig. 9) reveals that the photoelectron and Auger electron binding energies decrease upon substitution of the chloride for bromide and then iodide (for exact values, see Table 2). Thus, as the ligand is varied down Group 17, the Ga $3d_{5/2}$ binding energy decreases as the electronegativity of the halogen decreases and the gallium atom becomes more electron rich. A similar trend was observed in a study of nickel(II) halides by XPS.³¹ Additionally, experimental and theoretical studies have demonstrated decreasing Lewis acidity for GaX₃ compounds while descending Group 17.⁵² All of the gallium trihalides exhibit sharp signals, as evidenced by small FWHM values (Table 2), and satisfactory correlations between the fitted and the experimental spectra were obtained.

The gallium XPS spectra for Ga_(m), GaNacNac^{Dipp}, Ga₂Cl₄(diox)₂ and GaCl₃, with oxidation numbers of 0, +1, +2 and +3, respectively, are shown in Fig. 10. The spectra reveal a marked shift in the binding energies. For example, the binding energy of the Ga $3d_{5/2}$ signal increases by approximately 2 eV between GaNacNac^{Dipp} and Ga₂Cl₄(diox)₂, and by approximately 1 eV between Ga₂Cl₄(diox)₂ and GaCl₃ and between Ga_(m) and GaNacNac^{Dipp} (Table 2). It becomes increasingly more difficult to remove an electron as one progresses from Ga_(m) to GaCl₃, presumably because the gallium becomes more electron deficient from gallium metal (0) to GaCl₃ (+3), which is in agreement with the assigned oxidation numbers for these compounds. Despite the changes

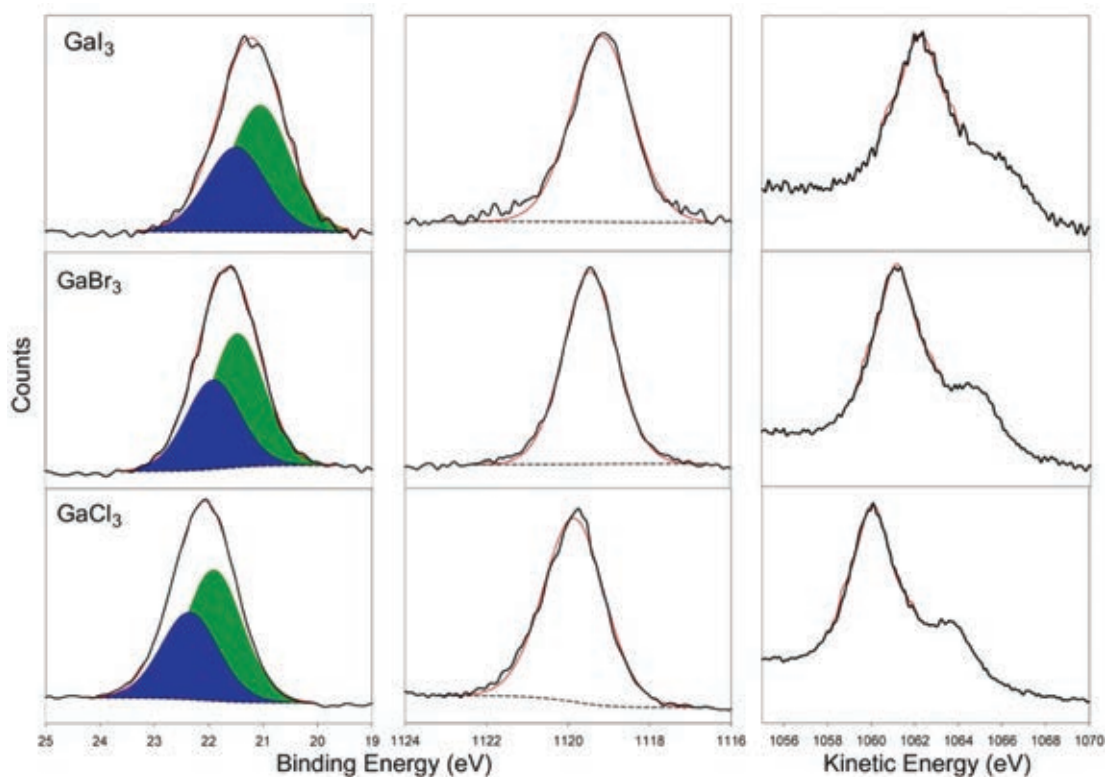


Fig. 9 Ga $3d$ (left), Ga $2p_{3/2}$ (center) and Ga $L_3M_{45}M_{45}$ (right) XPS spectra of GaCl₃ (bottom), GaBr₃ (middle) and GaI₃ (top).

Table 2 Photoelectron binding and Auger electron kinetic energies and full-width at half-maxima for high-resolution XPS spectra

Compound	Peak	Binding or kinetic energy (eV)	FWHM (eV)
Ga _(m)	Ga 3d _{5/2}	18.39	0.57
	Ga 2p _{3/2}	1116.49	1.04
	Ga L ₃ M ₄₅ M ₄₅	1068.01	0.79
GaNacNac ^{Dipp} 4	Ga 3d _{5/2}	19.29	1.74
	Ga 2p _{3/2}	1117.50	2.27
	Ga L ₃ M ₄₅ M ₄₅	1063.09	2.05
K[GaDAB ^{Dipp}] 5	Ga 3d _{5/2}	20.17	1.77
	Ga 2p _{3/2}	1118.02	2.18
	Ga L ₃ M ₄₅ M ₄₅	1061.92	1.78
[Ga(prismand)][OTf] 6	Ga 3d _{5/2}	21.34	1.24
	Ga 2p _{3/2}	1119.31	1.87
	Ga L ₃ M ₄₅ M ₄₅	1060.65	1.41
Ga ₂ Cl ₄ (diox) ₂ 7	Ga 3d _{5/2}	21.10	1.67
	Ga 2p _{3/2}	1118.86	2.13
	Ga L ₃ M ₄₅ M ₄₅	1061.39	2.16
Ga ₂ I ₄ (NH ₂ <i>t</i> Bu) ₂ 8	Ga 3d _{5/2}	20.53	1.64
	Ga 2p _{3/2}	1118.36	2.03
	Ga L ₃ M ₄₅ M ₄₅	1062.13	1.61
Ga ₂ I ₂ Ar ⁺ ₂ 9	Ga 3d _{5/2}	20.48	1.34
	Ga 2p _{3/2}	1118.33	1.93
	Ga L ₃ M ₄₅ M ₄₅	1063.01	2.20
GaCl ₃ 10	Ga 3d _{5/2}	21.91	1.23
	Ga 2p _{3/2}	1119.85	1.76
	Ga L ₃ M ₄₅ M ₄₅	1060.09	1.53
GaBr ₃ 11	Ga 3d _{5/2}	21.48	1.16
	Ga 2p _{3/2}	1119.45	1.53
	Ga L ₃ M ₄₅ M ₄₅	1061.17	1.51
GaI ₃ 12	Ga 3d _{5/2}	21.06	1.28
	Ga 2p _{3/2}	1119.17	1.76
	Ga L ₃ M ₄₅ M ₄₅	1062.26	1.57
GaCl ₂ Mes 13	Ga 3d _{5/2}	21.84	1.64
	Ga 2p _{3/2}	1120.10	1.94
	Ga L ₃ M ₄₅ M ₄₅	1060.16	1.92
Ga ₂ Cl ₄ 14	Ga 3d _{5/2}	21.77	1.34
	Ga 2p _{3/2}	1119.54	1.85
	Ga L ₃ M ₄₅ M ₄₅	1060.43	1.61
Ga ₂ I ₄ 15	Ga 3d _{5/2}	20.80	1.51
	Ga 2p _{3/2}	1118.72	2.08
	Ga L ₃ M ₄₅ M ₄₅	1061.98	2.06
Ga ₂ O ₃ 19	Ga 3d _{5/2}	20.00	1.22
	Ga 2p _{3/2}	1117.80	1.55
	Ga L ₃ M ₄₅ M ₄₅	1062.60	1.49
[Ga ₃ Cl ₄ (crypt-222)][GaCl ₄] 1	Ga 3d _{5/2}	20.79	1.63
	Ga 2p _{3/2}	1118.51	2.10
	Ga L ₃ M ₄₅ M ₄₅	1061.64	1.82
[Ga ₂ Cl ₂ (crypt-222)][OTf] ₂ 2	Ga 3d _{5/2}	20.65	1.61
	Ga 2p _{3/2}	1118.57	2.47
	Ga L ₃ M ₄₅ M ₄₅	1061.62	1.84
[Ga ₂ I ₂ (crypt-222)][GaI ₄] _{1.75} [OTf] _{0.25} 3	Ga 3d _{5/2}	21.00	1.19
	Ga 2p _{3/2}	1118.90	1.57
	Ga L ₃ M ₄₅ M ₄₅	1061.91	1.85

Ga L₃M₄₅M₄₅ signals are kinetic energy values, which have opposite trends to binding energies (eqn (1)).

in chemical state, the line shapes of each compound are similar, with narrow FWHM, although the signals for Ga_(m) are markedly more intense and have a much narrower FWHM (≤ 1.0 eV). The FWHM of the Ga L₃M₄₅M₄₅ signal of GaCl₃ is narrower by more than 0.5 eV compared to the FWHM values of GaNacNac^{Dipp} and Ga₂Cl₄(diox)₂. The trend is likely a result of the highly symmetric bonding environment in GaCl₃⁵³ in comparison to GaNacNac^{Dipp}⁵⁴ and Ga₂Cl₄(diox)₂, and therefore, is not related to the chemical state.⁵⁵

Wagner plots were generated to reveal further trends in the chemical state of the gallium centers as a function of ligand type and assigned oxidation number. The Ga 3d_{5/2} binding energies, Ga L₃M₄₅M₄₅ kinetic energies and the Auger parameter values for the gallium halides and compounds with an assigned oxidation number of +3 are shown in Fig. 11. As with nickel(II) halides,³¹ increasing Auger electron kinetic energy, decreasing photoelectron binding energy, and increasing Auger parameter values were observed as the halide

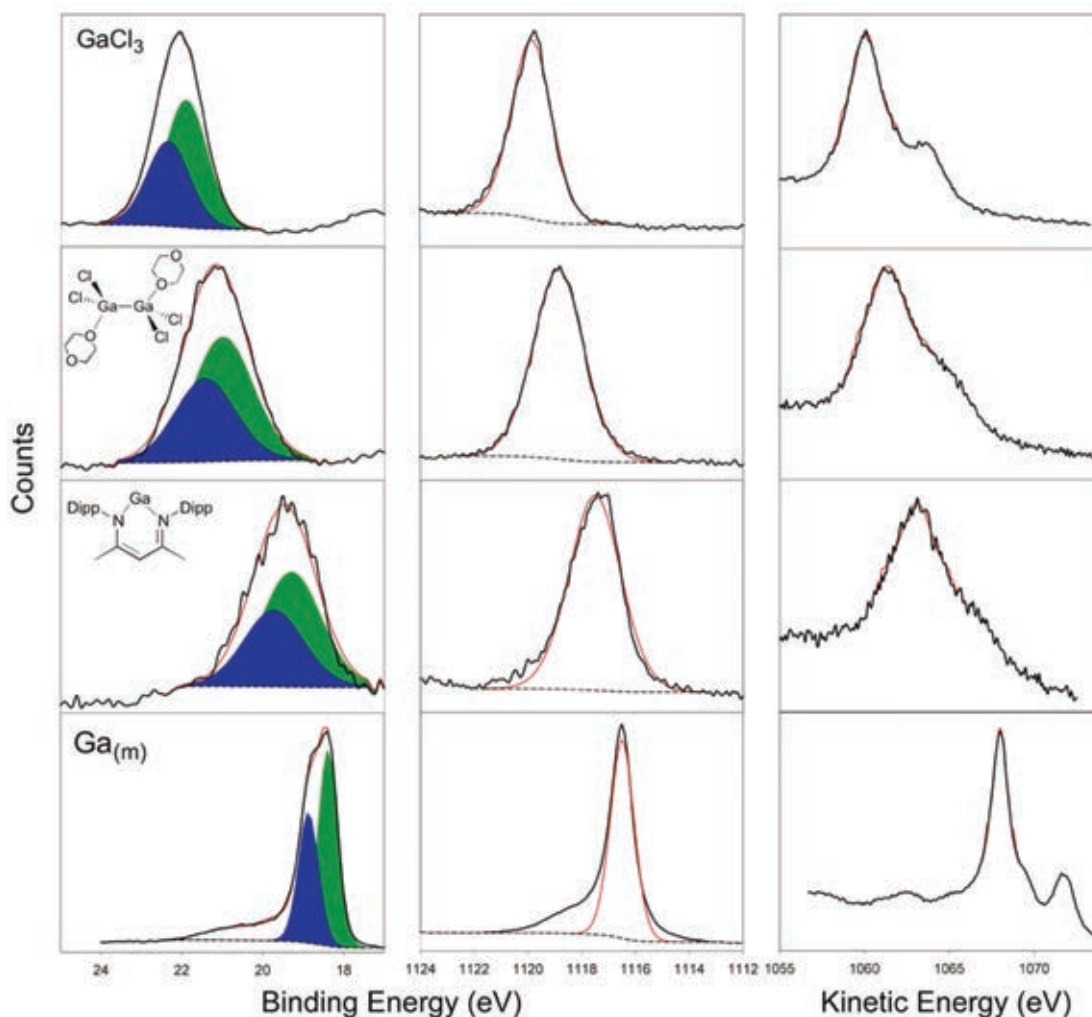


Fig. 10 Ga 3d (left), Ga 2p_{3/2} (center) and Ga L₃M₄₅M₄₅ (right) XPS spectra of Ga_(m) (bottom), GaNacNac^{Dipp} (lower middle), Ga₂Cl₄(diox)₂ (upper middle) and GaCl₃ (top).

ligands were altered down Group 17. The nearly linear increase with a slope approaching 2 in the Auger parameter values from GaCl₃ to GaBr₃ to GaI₃ suggests that gallium trihalides are not dominated by initial or final state effects. This is corroborated by the calculated initial and final state shifts for each compound (Table 3), where the initial state shifts for the gallium trihalides differ by 0.19 eV (from -1.32 eV for GaCl₃ to -1.13 eV for GaI₃), and the final state shifts differ by 0.66 eV (from -2.20 eV for GaCl₃ to -1.54 eV for GaI₃), which are small in comparison to nickel(II) halides, whose initial state shifts vary by 2.7 eV and final state shifts vary by 0.9 eV. The vast difference between the initial and final state shifts for nickel(II) halides lead to the conclusion that initial state effects dominate these compounds, but such a definitive trend was not apparent for the gallium trihalides.³¹

The gallium chlorides GaCl₃, GaCl₂Mes and Ga₂Cl₄, possess similar Auger parameters. Specifically, GaCl₃ and GaCl₂Mes are nearly identical, possibly resulting from a similar solid-state structure, with four coordinate gallium

atoms, and bridging chloride ligands.^{53,56} Electronically, both the chloride and mesityl ligands are electron withdrawing, and GaCl₃ and GaCl₂Mes demonstrate similar reactivity. Despite the solid-state structure of Ga₂Cl₄ having a gallium(I) cation and a tetrachlorogallate(III) anion ([Ga][GaCl₄]),¹² the signal was not broadened, as might be expected for a mixed valent salt. Given the known solid-state structure, three suggestions are put forward to rationalize the low FWHM: (1) upon X-ray irradiation, the gallium cation in [Ga][GaCl₄] undergoes disproportionation and is oxidized; (2) the cation is volatilized under the conditions of the experiment and not detected, which is supported by the observation of gallium in the survey spectra of subsequently analyzed samples unrelated to this study; or (3) unlike the gallium(I) in GaNacNac^{Dipp}, the gallium(I) in [Ga][GaCl₄] is, essentially, a naked cation carrying a full positive charge and stabilized in the solid-state only by interactions with the chloride ligands of the tetrachlorogallate(III) anion.¹² Similar interactions are observed in the solid-state structure of GaCl₃.⁵³ Thus, the cationic gallium(I) has a

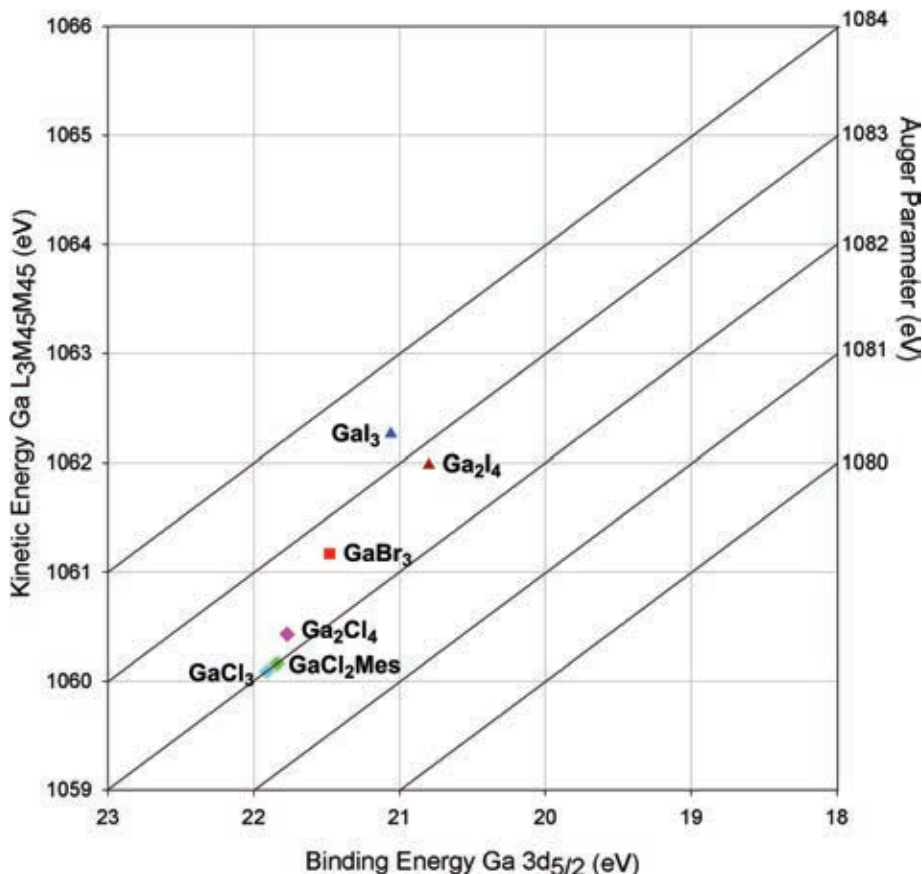


Fig. 11 Wagner plot of gallium halides using Ga 3d_{5/2} binding energy. Symbol legend: diamond = chloride ligands; square = bromide ligands; triangle = iodide ligands.

Table 3 Auger parameters and relevant shifts for compounds analyzed using Ga 3d_{5/2} binding energy

Compound	Auger parameter, α' (eV)	ΔE_B (eV)	ΔE_K (eV)	Relaxation shift, $\Delta\alpha'$ (eV)	Final state shift, ΔR (eV)	Initial state shift, $\Delta\epsilon$ (eV)
Ga _(m) (meas)	1086.40	—	—	—	—	—
Ga _(m) (lit) ^{47–49}	1086.69	—	—	—	—	—
GaNacNac ^{Dipp}	1082.38	0.90	-4.92	-4.02	-2.01	1.11
K[GaDAB ^{Dipp}]	1081.84	1.84	-6.40	-4.56	-2.28	0.44
[Ga(prismand)] [OTf]	1081.99	2.95	-7.36	-4.41	-2.21	-0.75
Ga ₂ Cl ₄ (diox) ₂	1082.39	2.61	-6.62	-4.01	-2.01	-0.61
Ga ₂ I ₄ (NH ₂ tBu) ₂	1082.66	2.14	-5.88	-3.74	-1.87	-0.27
Ga ₂ I ₂ Ar ⁺ ₂	1083.49	2.09	-5.00	-2.91	-1.46	-0.64
GaCl ₃	1082.00	3.52	-7.92	-4.40	-2.20	-1.32
GaBr ₃	1082.65	3.09	-6.84	-3.75	-1.88	-1.22
GaI ₃	1083.32	2.67	-5.75	-3.08	-1.54	-1.13
GaCl ₂ Mes	1082.00	3.45	-7.85	-4.40	-2.20	-1.25
Ga ₂ Cl ₄	1082.20	3.38	-7.58	-4.20	-2.10	-1.28
Ga ₂ I ₄	1082.78	2.41	-6.03	-3.62	-1.81	-0.60
GaN	1084.05	1.21	-3.56	-2.35	-1.18	-0.35
GaP	1085.33	0.91	-1.98	-1.07	-0.54	-0.38
GaAs	1085.77	0.81	-1.44	-0.63	-0.32	-0.49
Ga ₂ O ₃ (meas)	1082.60	1.61	-5.41	-3.80	-1.90	0.29
Ga ₂ O ₃ (lit) ^{36,47}	1082.85	2.01	-5.56	-3.55	-1.78	-0.24
Ga ₂ Se ₃	1085.20	1.41	-2.61	-1.20	-0.60	-0.81
1	1082.43	2.40	-6.37	-3.97	-1.99	-0.42
2	1082.27	2.26	-6.39	-4.13	-2.07	-0.20
3	1082.91	2.61	-6.10	-3.49	-1.75	-0.87

Calculations were performed as follows using the measured data for Ga_(m): $\alpha' = E_B + E_K(\text{Auger})$; $\Delta E_B = E_B - E_B(\text{Ga}_{(m)})$; $\Delta E_K = E_K(\text{Auger}) - E_K(\text{Auger}, \text{Ga}_{(m)})$; $\Delta\alpha' = \alpha' - \alpha'(\text{Ga}_{(m)}) = 2\Delta R$; $\Delta\epsilon = -\Delta E_B - \Delta R$.

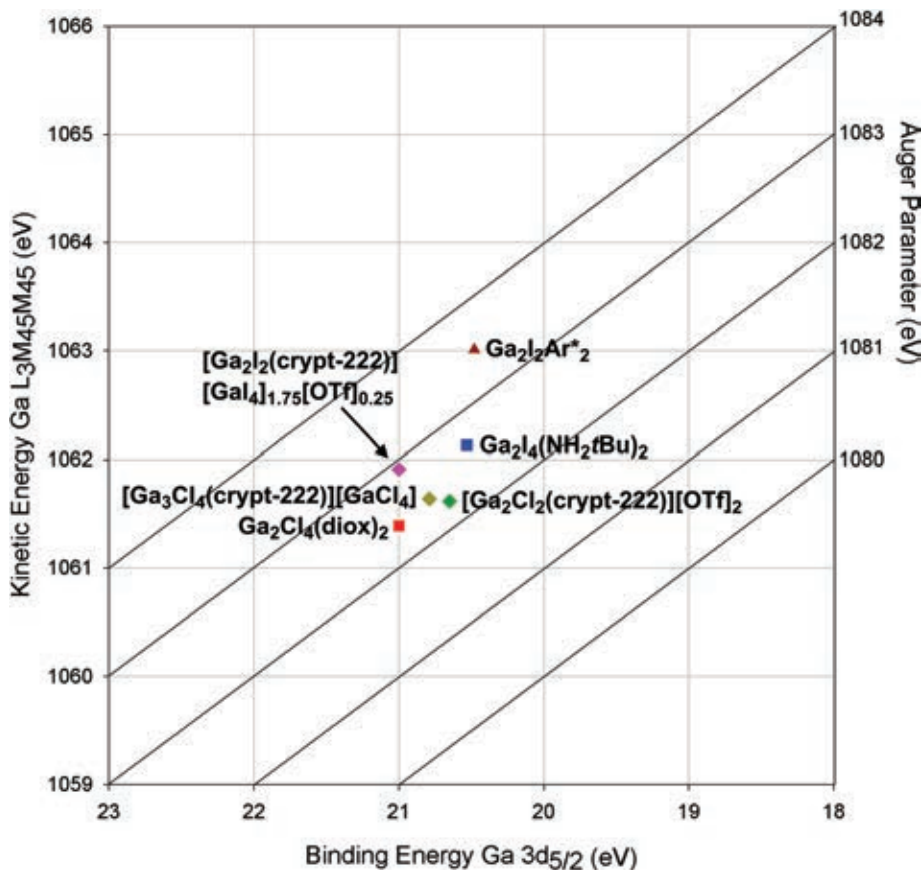


Fig. 12 Wagner plot of Ga–Ga compounds using Ga 3d_{5/2} binding energy. Symbol legend: diamond = synthesized gallium–cryptand complexes; square = chloride and iodide ligands and O/N donors; triangle = iodide and terphenyl ligands.

chemical state similar to a gallium(III) with covalently bound ligands leading to a single signal and the observed location for [Ga][GaCl₄] on the Wagner plot. The data obtained for [Ga][GaCl₄] also reveal a higher Auger parameter (0.2 eV), with lower binding and higher kinetic energies, than GaCl₃ and GaCl₂Mes, suggesting that the presence of the additional chloride ligand on the tetrachlorogallate anion increases the electron density at the gallium center.

As with Ga₂Cl₄, the FWHM of the Ga 3d_{5/2} and 2p_{3/2} signals of Ga₂I₄ ([Ga][GaI₄]) were both less than 2.1 eV, indicating either a single species or multiple species with similar chemical states were present in the sample. As with the gallium trihalides, the gallium in the iodo derivative of Ga₂X₄ is more electron rich compared to the analogous chloro derivative. However, unlike [Ga][GaCl₄] and GaCl₃, the Auger parameter for [Ga][GaI₄] was lower than that for GaI₃. For both [Ga][GaCl₄] and [Ga][GaI₄], the photoelectron binding energies decrease compared to the corresponding GaX₃; however, the Auger electron kinetic energy increases going from [Ga][GaCl₄] to GaCl₃ and decreases going from [Ga][GaI₄] to GaI₃, demonstrating the large, but subtle, effect the electronic properties of the ligands can have on the chemical state of the gallium center.

A Wagner plot for the gallium compounds containing a Ga–Ga bond and an oxidation number of +2 is presented in Fig. 12. Ga₂Cl₄(diox)₂ is more electron deficient than Ga₂I₄(NH₂tBu)₂, with chloride being more electronegative than iodide and amines being better donors than ethers, decreasing the binding energy for the iodide derivative.⁵⁷ As with the gallium trihalides, a trendline with a slope approaching 2 is observed going from Ga₂Cl₄(diox)₂ to Ga₂I₄(NH₂tBu)₂ and to Ga₂I₂Ar*₂. The increase in the Auger parameter from Ga₂I₄(NH₂tBu)₂ to Ga₂I₂Ar*₂ is mostly induced by an increase in the Auger electron kinetic energy. As the photoelectron binding energy does not undergo a significant shift, the gallium centers in both compounds must have a similar chemical state. The change in the Auger electron kinetic energy must result from an undetermined phenomenon after the initial ionization occurs in Ga₂I₂Ar*₂. For compounds with a gallium oxidation number of +3 (Fig. 11) and +2 (Fig. 12), it appears that the expectation that final state effects are more influential than initial state effects is not observed within each oxidation number as the Auger parameters differ significantly as the ligands are varied for gallium compounds with higher assigned oxidation numbers unlike for the aforementioned copper compounds.³³

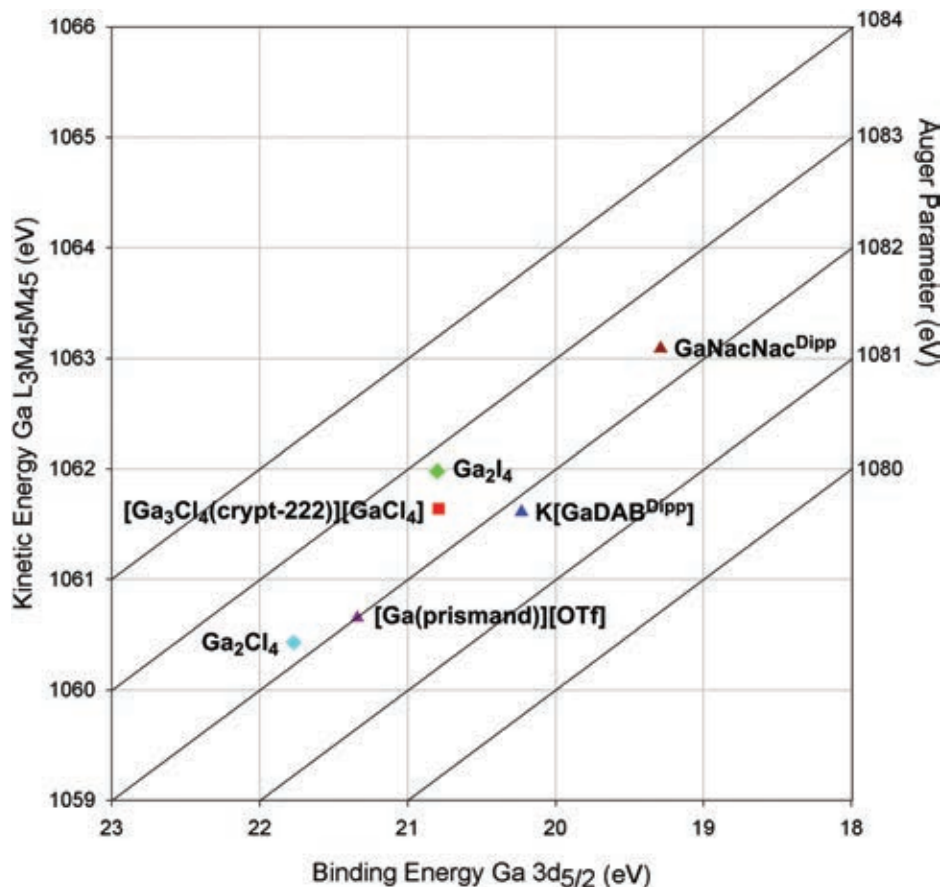


Fig. 13 Wagner plot of Ga(I) compounds using Ga $3d_{5/2}$ binding energy. Symbol legend: diamond = halide ligands; square = chloride ligands and O/N donors; triangle = organic ligands.

Fig. 13 shows the Wagner plot generated for gallium compounds with an oxidation number of +1. Although $\text{GaNacNac}^{\text{Dipp}}$, $\text{K[GaDAB}^{\text{Dipp}}]$ and $[\text{Ga}(\text{prismand})][\text{OTf}]$ are classified as having the same oxidation number, they have significantly different Auger and photoelectron energies but similar Auger parameter values. The structures of $\text{GaNacNac}^{\text{Dipp}}$ and $\text{K[GaDAB}^{\text{Dipp}}]$ are somewhat related, as they both possess anionic bidendate nitrogen ligands, however, the dianionic nature of the $[\text{DAB}^{\text{Dipp}}]^{2-}$ ligand leads to the coordination of a potassium counter-ion to the gallium center in $\text{K[GaDAB}^{\text{Dipp}}]$, and thus, the gallium atom donates some of its electron density to the potassium cation, giving it a higher Ga $3d_{5/2}$ binding energy than $\text{GaNacNac}^{\text{Dipp}}$. Similar to $[\text{Ga}][\text{GaCl}_4]$, the $[\text{Ga}(\text{prismand})]^+$ moiety in $[\text{Ga}(\text{prismand})][\text{OTf}]$ is cationic with weak interactions between the neutral prismand macrocycle and the gallium, and thus, the gallium is more electron deficient in comparison to those complexes with covalent bidendate nitrogen ligands, leading to a lowering of the Ga $L_3M_{45}M_{45}$ kinetic energy, and an increase in the Ga $3d_{5/2}$ binding energy. The Auger parameter for $[\text{Ga}(\text{prismand})][\text{OTf}]$ is similar to that of $[\text{Ga}][\text{GaCl}_4]$, where the gallium cation is also weakly stabilized and electron deficient. Despite the differences in the structures of the

gallium compounds with an oxidation number of +1, they appear to have similar final state effects, as they all possess Auger parameter values of approximately 1082 eV, varying by only 0.27 eV. Thus, the chemical states of these gallium compounds are more influenced by the nature of the attached ligands, and the polarization of the gallium centers upon ionization must be similar. The gallium in $[\text{Ga}(\text{prismand})][\text{OTf}]$ is similar in chemical state to the gallium trihalides (GaX_3) and would, therefore, be expected to act as a Lewis acid. Conversely, $\text{GaNacNac}^{\text{Dipp}}$ and $\text{K[GaDAB}^{\text{Dipp}}]$ are much more electron rich, and would be expected to act as Lewis bases, as well as being less reactive toward electron donors. Indeed, the Lewis basic nature of $\text{GaNacNac}^{\text{Dipp}}$ and $\text{K[GaDAB}^{\text{Dipp}}]$ is well-known.^{58,59} Finally, the difference in position on the Wagner plot between $\text{GaNacNac}^{\text{Dipp}}$ and $\text{K[GaDAB}^{\text{Dipp}}]$ can be attributed to the coordination of the potassium cation in the latter compound, decreasing the electron-richness of the gallium center. The preceding analysis demonstrates how Wagner plots are effective at the prediction of reactivity pathways for novel main group compounds and can be a useful tool in the classification of chemical states.

Fig. 14 gives the Wagner plot for selected gallium complexes stabilized by chlorine and/or nitrogen-based ligands of

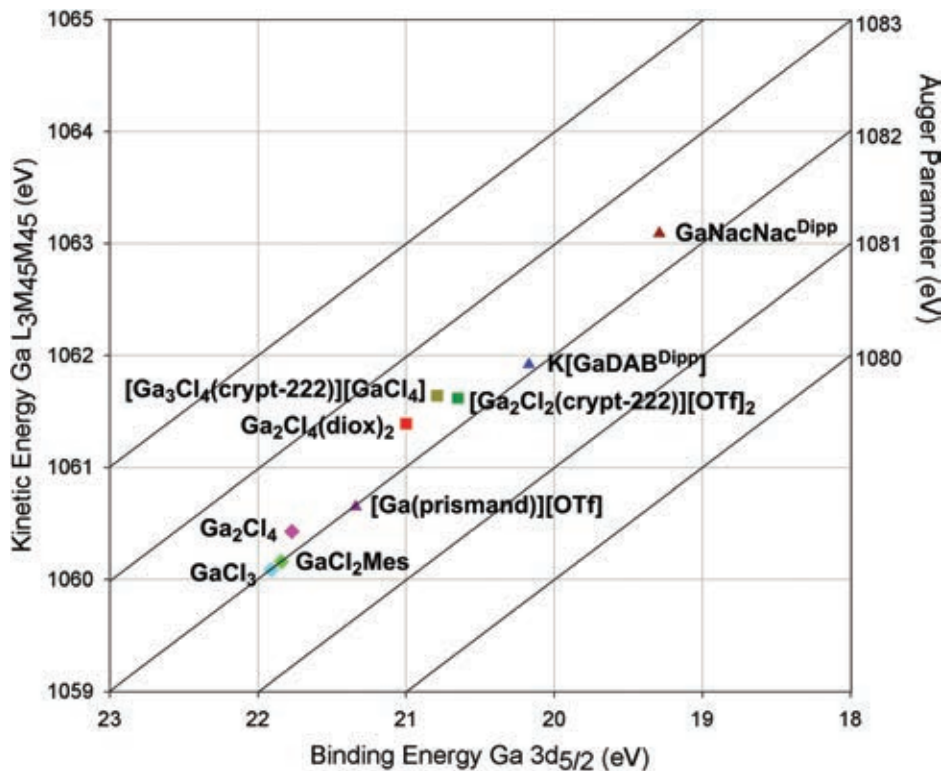


Fig. 14 Wagner plot of gallium–chloride and gallium–nitrogen compounds using Ga $3d_{5/2}$ binding energy. Symbol legend: diamond = Ga(III); square = Ga(II); triangle = Ga(I).

all oxidation numbers. It is evident that the Auger parameters are all very similar, leading to the generation of a trendline with a slope of approximately 1, indicating that, for this series of compounds, similar final state effects are observed whereas the initial state effects differ significantly ($\Delta(\Delta R) = 0.28$ eV; $\Delta(\Delta E) = 2.43$ eV). Again, the similarity of the final state effects can be understood on the basis of the nature of the ligands; chloride and nitrogen are both hard bases,³ with minimal polarizability and little effect on the polarizability of the gallium. However, their effect on the gallium centers can be observed in the significant initial state shifts. Three distinct regions of the Wagner plot can be identified in Fig. 14. The bottom left area of the plot with $\text{Ga } L_3M_{45}M_{45} \leq 1061$ eV and $\text{Ga } 3d_{5/2} \geq 21.5$ eV, correlates to the most electron deficient gallium complexes often with an oxidation number of +3. An intermediate area is present in the center of the plot ($1061 \leq \text{Ga } L_3M_{45}M_{45} \leq 1062$ eV and $21.5 \geq \text{Ga } 3d_{5/2} \geq 20.5$ eV), where most compounds with an oxidation number of +2 and the gallium–cryptand complexes are located. Toward the upper right of the plot ($\text{Ga } L_3M_{45}M_{45} \geq 1062$ eV; $\text{Ga } 3d_{5/2} \leq 20.5$ eV), electron-rich gallium compounds that are in the +1 oxidation number can be found. Not only can the oxidation numbers be determined using this method, these data allow for a classification of the complexes on the basis of their chemical states. Furthermore, analogous reactivity might be expected from complexes with gallium in similar chemical states. The ability of XPS to differentiate clearly between multiple chemical states of molecular gallium compounds is a striking

result, as this technique is widely accessible, although sparingly used, for this purpose. Furthermore, since XPS is widely accessible, our results suggest that this technique can be easily applied to the study of other main group molecular complexes to aid in the understanding of their electronic nature and reactivity.

The Wagner plot for gallium–iodide complexes, shown in Fig. 15, does not appear to have distinct groupings as a function of ligand or oxidation number. Unlike the chloride-containing complexes, a trendline cannot be generated for the gallium–iodide compounds and it is unclear whether initial or final state effects dominate. This could be due to the increased number of electrons in iodide ligands in comparison to chloride, where it is able to donate more electron density to the gallium center in gallium–iodide compounds, limiting the shifts in binding energy of the gallium centers. The polarizability of iodine, with its diffuse electron cloud could also contribute to the inconsistency of the Auger parameter for gallium–iodide complexes. Notably, compounds with different oxidation numbers ($\text{Ga}_2\text{I}_4(\text{NH}_2t\text{Bu})_2$, $[\text{Ga}_2\text{I}_2(\text{crypt-222})][\text{GaI}_4]_{1.75}[\text{OTf}]_{0.25}$ compared to $[\text{Ga}][\text{GaI}_4]$ and GaI_3) are in close proximity, which demonstrates that although the four compounds are classified differently based on their assigned oxidation numbers, the experimentally determined chemical states of the gallium centers indicate they are all very similar in nature and should exhibit similar reactivity. Once again, the formalism of oxidation or valence numbers fails to accurately describe the chemical state of a given element which may lead

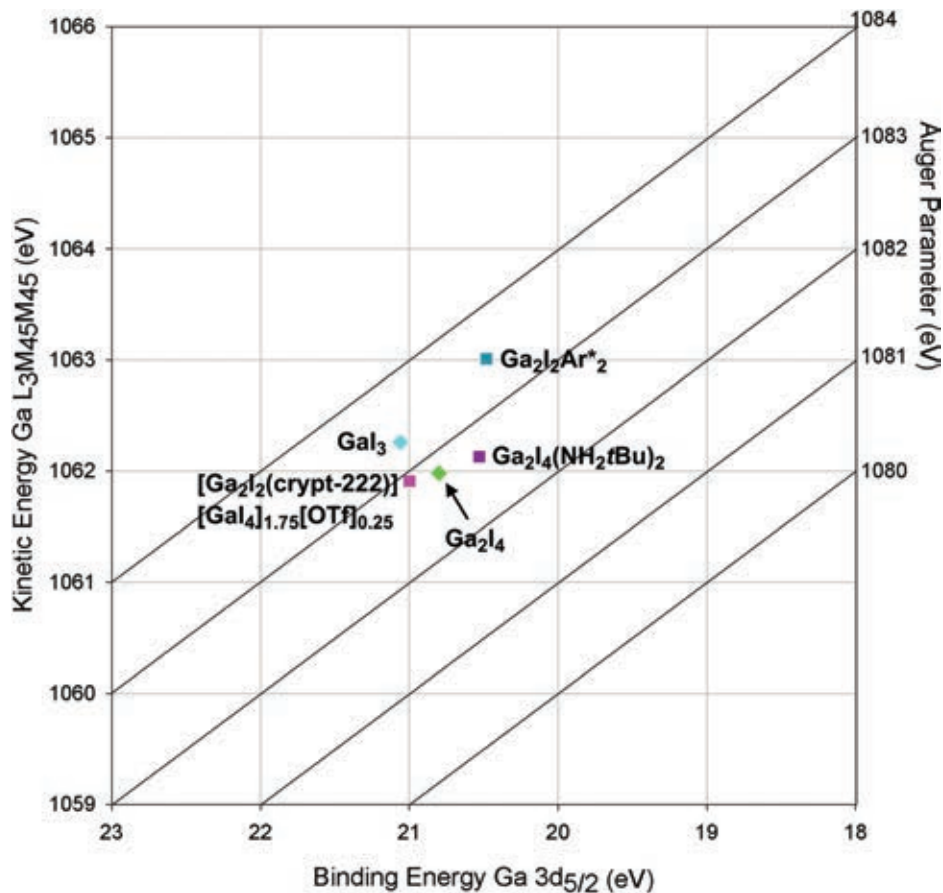


Fig. 15 Wagner plot of gallium-iodide compounds using Ga $3d_{5/2}$ binding energy. Symbol legend: diamond = Ga(III); square = Ga(II).

to misconceptions of the reactivity. Not surprisingly, experimental determinations of chemical states are more appropriate and should lead to more accurate predictions of reactivity.²

As shown in Fig. 14 and 15, the data points for $[\text{Ga}_3\text{Cl}_4(\text{crypt-222})][\text{GaCl}_4]$, $[\text{Ga}_2\text{Cl}_2(\text{crypt-222})][\text{OTf}]_2$ and $[\text{Ga}_2\text{I}_2(\text{crypt-222})][\text{GaI}_4]_{1.75}[\text{OTf}]_{0.25}$ fall within the intermediate section of the Wagner plot. An oxidation number of +2 for $[\text{Ga}_2\text{Cl}_2(\text{crypt-222})][\text{OTf}]_2$ and its iodide-substituted analogue is consistent with the solution-state NMR spectroscopic data and computational data, where both gallium centers are equivalent and each have a charge of +1. Other compounds with similar connectivity are located in this area of the Wagner plot. The proximity of the data points for both $[\text{Ga}_2\text{Cl}_2(\text{crypt-222})][\text{OTf}]_2$ and $[\text{Ga}_2\text{I}_2(\text{crypt-222})][\text{GaI}_4]_{1.75}[\text{OTf}]_{0.25}$ on the Wagner plot indicates that the macrocyclic ether ligand has a stronger influence on the Auger parameter compared to the halide ligands attached to the gallium center. Despite the presence of an additional gallium environment, namely the tetraiodogallate(III) anion, the location of $[\text{Ga}_2\text{I}_2(\text{crypt-222})][\text{GaI}_4]_{1.75}[\text{OTf}]_{0.25}$ on the Wagner plot it is not significantly different from the positions of the other two gallium-cryptand[2.2.2] complexes.

While the dicationic nature of the $[\text{Ga}_2\text{X}_2(\text{crypt-222})]^{2+}$ complexes might be expected to result in significant electron

deficiency at the gallium centers, they are positioned within the intermediate region of the Wagner plot (Fig. 14). Although XPS data of the precursor to $[\text{Ga}_2\text{X}_2(\text{crypt-222})]^{2+}$, $\text{Ga}_2\text{Cl}_4(\text{THF})_2$, was not obtained due to its poor stability,^{13,60} the THF complex is analogous to $\text{Ga}_2\text{Cl}_4(\text{diox})_2$, which also contains a $\text{Cl}_2\text{GaGaCl}_2$ core stabilized by ether donors. $\text{Ga}_2\text{Cl}_4(\text{diox})_2$ is located in close proximity to the two $[\text{Ga}_2\text{X}_2(\text{crypt-222})]^{2+}$ dications on the Wagner plot in Fig. 14, suggesting that upon removal of halide ligands and coordination of cryptand[2.2.2], the chemical state of the gallium does not significantly differ from $\text{Ga}_2\text{Cl}_4(\text{diox})_2$, and therefore, from the $\text{Ga}_2\text{Cl}_4(\text{THF})_2$ precursor. The Auger parameters for both dications are slightly elevated from $\text{Ga}_2\text{Cl}_4(\text{diox})_2$ due to the effective coordination of the multidentate cryptand[2.2.2] donor; the gallium centers are more electron rich in these compounds, resulting in higher Auger electron kinetic energies, and lower photoelectron binding energies. This is quite striking, as upon initial scrutiny of the gallium-cryptand[2.2.2] complexes, it is not immediately obvious that the gallium centers in these cations would be more electron rich than the starting materials given the charge assigned to the gallium centers.

While several of the postulated bonding models for $[\text{Ga}_3\text{Cl}_4(\text{crypt-222})]^+$ suggested that it may have at least one

gallium(i) center, this is not reflected in the XPS data on the basis of its Auger parameter, which was greater than those of $\text{GaNaCNac}^{\text{DiPP}}$ and $\text{K}[\text{GaDAB}^{\text{DiPP}}]$, and its position near the center of the Wagner plot in Fig. 14. While structural data for $[\text{Ga}_3\text{Cl}_4(\text{crypt-222})][\text{GaCl}_4]$ demonstrated four structurally unique gallium atoms, only one signal was observed in the XPS spectrum. The resolution of the experiment is limited by the natural line width of the gallium signals²⁸ and individual environments may not be resolved, however, if multiple gallium environments were present, the signal would be expected to be broad. The signals for $[\text{Ga}_3\text{Cl}_4(\text{crypt-222})][\text{GaCl}_4]$ are narrow with FWHM between 1.63 and 2.10 eV, consistent in magnitude with the FWHM of other compounds possessing only one unique gallium environment and suggesting that all gallium atoms in the complex have similar chemical states despite the variation in coordinating ligands.¹⁷ On the basis of the XPS data, the chemical state of $[\text{Ga}_3\text{Cl}_4(\text{crypt-222})]^+$ most closely resembles compounds with an oxidation number of +2, and would, therefore, be expected to react similarly to $\text{Ga}_2\text{Cl}_4(\text{diox})_2$ and $\text{Ga}_2\text{I}_4(\text{NH}_2t\text{Bu})_2$. The same trend was also observed for the $[\text{Ga}_2\text{X}_2(\text{crypt-222})]^{2+}$ complexes. Thus, in comparison to $\text{Ga}_2\text{Cl}_4(\text{diox})_2$, all three gallium–cryptand complexes are expected to act as electrophiles, and may react with a variety of Lewis bases and

nucleophiles, however, such reactivity may be impeded by the bulkiness of the cryptand ligand. Once again, the ability of XPS to allow for more precise reactivity predictions compared to qualitative descriptors is evident.

As a significant amount of XPS data have been reported for a variety of solid-state gallium materials, a Wagner plot for the gallium materials is presented in Fig. 16. The Auger parameter values were obtained by averaging all of the data available for each compound in the NIST XPS database.^{36–44,47–51,56} A sample of Ga_2O_3 was analyzed in this study to determine whether the analytical methods used in this study were within experimental error of the data reported. Although some variation was observed between the data obtained experimentally for Ga_2O_3 and that reported in the literature,^{36,39,47,48} the difference in the Ga $3d_{5/2}$ binding energy was approximately 0.4 eV, which falls within experimental error.²⁸

Similar to the trends observed for the gallium trihalides, trendlines with large slopes were evident for Ga(Group 15) and Ga_2 (Group 16)₃ materials. The slopes were larger than for the gallium trihalides, and demonstrate that for both Group 15 and 16 gallium materials, initial state shifts do not change nearly as much as the final state shifts upon descending the group, especially for Group 16 (Group 15: $\Delta(\Delta R) = 0.86$ eV;

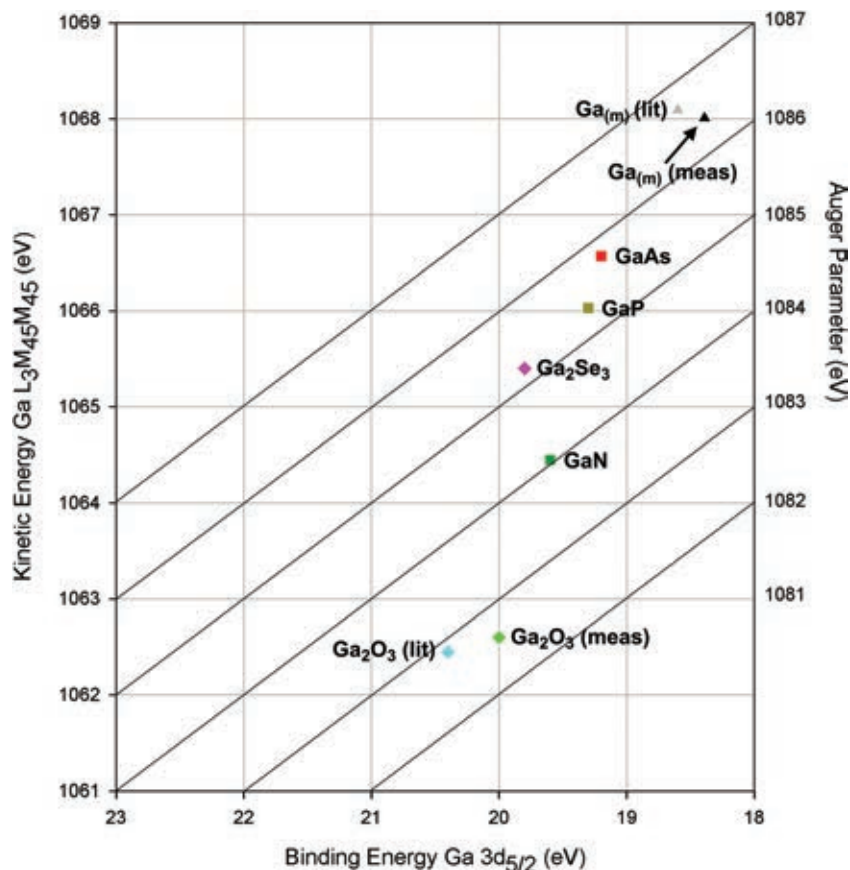


Fig. 16 Wagner plot of gallium materials using Ga $3d_{5/2}$ binding energy. Symbol legend: diamond = Group 15 elements; square = Group 16 elements.

$\Delta(\Delta\epsilon) = 0.46$ eV; Group 16: $\Delta(\Delta R) = 3.34$ eV; $\Delta(\Delta\epsilon) = 1.1$ eV). Thus, final state effects dominate for these materials, which demonstrates that the nature of the Group 15 or 16 elements has a vast influence on the electronic properties of the material, specifically following ionization. Interestingly, the location of the gallium materials on the Wagner plot is close to gallium metal. All of the materials shown in Fig. 16 except Ga_2O_3 have significantly elevated Auger parameters in comparison to the molecular gallium compounds (≥ 1084 eV for the gallium materials; ≤ 1083 eV for molecular compounds), despite the gallium in each of the compounds having an oxidation number of +3. The Ga $3d_{5/2}$ binding energies are lowered significantly, and suggest that these materials are alloy-like, with significant electron mobility. This is indeed the case for the Group 15 materials, as gallium nitride, phosphide and arsenide are all semiconductors used in the electronics industry.⁶¹ Additionally, as the atomic number of the Group 15 element increases, the bonding becomes more metallic; the relative size of arsenic and gallium are more similar compared to nitrogen and gallium. Given the position of GaAs on the Wagner plot, clearly the individual atoms are more elemental in nature, and more closely related to gallium metal in terms of their electron richness, than to the electron deficient gallium trihalides. A similar trend is observed for the Group 16 gallium materials. Ga_2O_3 is a wide gap semiconductor and an important industrial material.⁶² When selenium is substituted for oxygen, the material, Ga_2Se_3 , becomes more alloy-like.

Similar Wagner plots were generated using the Ga $2p_{3/2}$ signal and compared to those generated using the Ga $3d_{5/2}$ signal. The Ga $2p_{3/2}$ Wagner plots are presented in the ESI (Fig. S1–S5†). The same trends were observed, including a slope approaching 3 for the gallium trihalides, indicating final state effects varied for GaX_3 compounds, and initial state effects did not, which is more pronounced than for the Ga $3d_{5/2}$ photoemission ($\Delta(\Delta R) = 0.73$ eV; $\Delta(\Delta\epsilon) = 0.11$ eV). As for the Ga $2p_{3/2}$ transition of the selected gallium–chloride and –nitrogen compounds, the trendline with a slope of approximately 1 and the initial and final state shifts ($\Delta(\Delta R) = 0.20$ eV; $\Delta(\Delta\epsilon) = 2.35$ eV) were similar to those observed with the Ga $3d_{5/2}$ data. While some of the Auger parameter data points were more dispersed in the Ga $2p_{3/2}$ data, for example, in the gallium–chloride compounds, some overlap was observed (Fig. S5†). Although the gap between the electron deficient and intermediate regions of the Wagner plot were more pronounced for the Ga $2p_{3/2}$ data, the intermediate and electron rich regions overlapped, suggesting that the Ga $3d_{5/2}$ data are more useful for chemical speciation as expected, due to the increased sensitivity of the Ga $3d_{5/2}$ signal to small changes experienced by the valence electrons.

Conclusion

In conclusion, we have performed XPS studies on a series of molecular gallium compounds with varying ligands and

chemical environments. The photoelectron emissions of the Ga $3d_{5/2}$ and Ga $2p_{3/2}$ core electrons were measured, as well as the Auger electron Ga $L_3M_{4,5}M_{4,5}$ emissions. Auger parameters were calculated and Wagner plots were generated which allowed for the chemical state determination of $[\text{Ga}_3\text{Cl}_4(\text{crypt-222})][\text{GaCl}_4]$ (1), $[\text{Ga}_2\text{Cl}_2(\text{crypt-222})][\text{OTf}]_2$ (2) and $[\text{Ga}_2\text{I}_2(\text{crypt-222})][\text{GaI}_4]_{1.75}[\text{OTf}]_{0.25}$ (3). The XPS data demonstrate that the cations of 1–3 are in an intermediate chemical state, which was not possible using other experimental and computational data. The data also reveal that for 1, although a single bonding model could not describe the bonding of the gallium centers of $[\text{Ga}_3\text{Cl}_4(\text{crypt-222})]^+$, which was demonstrated in the previously obtained data, it exists in an intermediate chemical state that is very similar to the other gallium–cryptand cations. The gallium trihalides have similar initial state effects, whereas gallium–chloride and –nitrogen complexes have similar final state effects. For molecular gallium complexes of different chemical states, namely electron rich and electron deficient, each were sufficiently separated to allow for the chemical state determination of these compounds. We have demonstrated the applicability of XPS to assess the chemical states of a variety of novel main group complexes giving valuable insights into the reactivity.

Experimental

General considerations

All manipulations were performed under an inert atmosphere of argon using general Schlenk techniques or under an atmosphere of nitrogen in an MBraun glovebox unless otherwise stated. All solvents were purified using an Innovative Technologies 400-5 Solvent Purification System and were stored over activated 3 or 4 Å molecular sieves, unless otherwise stated. All reagents were used as received from Sigma-Aldrich, Alfa Aesar, Strem Chemicals or Gelest. Commercially available compounds (GaCl_3 , Strem; GaBr_3 , Alfa Aesar; GaI_3 , Gelest; Ga_2O_3 , Alfa) were used as received. GaI^+ ,⁶³ $[\text{Ga}_3\text{Cl}_4(\text{crypt-222})][\text{GaCl}_4]$ (1), $[\text{Ga}_2\text{Cl}_2(\text{crypt-222})][\text{OTf}]_2$ (2),¹⁷ $\text{GaNacNac}^{\text{Dipp}}$ (4),⁵⁴ $\text{K}[\text{GaDAB}^{\text{Dipp}}]$ (5),⁶⁴ $\text{Ga}_2\text{Cl}_4(1,4\text{-dioxane})_2$ (7),⁵⁵ $\text{Ga}_2\text{I}_4(\text{NH}_2^t\text{Bu})_2$ (8),⁶⁵ $\text{Ga}_2\text{I}_2(2,6\text{-dimesitylphenyl})_2$ (9),⁶⁶ GaCl_2Mes (13),⁶⁷ Ga_2Cl_4 (14),^{68,69} and Ga_2I_4 (15)⁶⁸ were synthesized according to literature procedures. The purity of the synthesized compounds was determined using ^1H , ^{19}F , and ^{71}Ga NMR spectroscopy. To avoid any potential contamination or oxidation of the air sensitive compounds, the samples were stored in air-tight, capped vials with fluoropolymer linings. The vials were further sealed using parafilm and tape. The vials were then transported to the XPS instrument and were opened and prepared in a purged argon-filled glove box, which was directly attached to the introduction chamber of the XPS instrument. NMR spectra were recorded on a Varian INOVA I400 (^1H 400 MHz; $^{13}\text{C}\{^1\text{H}\}$ 101 MHz; ^{19}F 376 MHz) or a Varian INOVA I600 (^1H 600 MHz; $^{13}\text{C}\{^1\text{H}\}$ 151 MHz; ^{19}F 565 MHz; ^{71}Ga 183 MHz) FTNMR spectrometer. Chemical shifts (δ) are reported in ppm and were internally referenced to the residual

protonated solvent peaks for ^1H spectra, and the deuterated solvent for $^{13}\text{C}\{^1\text{H}\}$ spectra. ^{19}F NMR spectra were referenced to CFCl_3 (0.0 ppm) based on the internal lock signal from the deuterated solvent and to $\text{Ga}(\text{NO}_3)_3$ (0.0 ppm) in D_2O for ^{71}Ga spectra. Coupling constants (J) are reported in Hz and multiplicities are reported as singlet (s), doublet (d), triplet (t), quartet (q), multiplet (m), broad (br) and overlapping (ov). Electrospray ionization mass spectra were collected using a Bruker micrOTOF II spectrometer. Mass spectral data are reported in mass-to-charge units (m/z).

Synthesis

Synthesis of $[\text{Ga}_2\text{I}_2(\text{crypt-222})][\text{GaI}_4]_{1.75}[\text{OTf}]_{0.25}$, 3. Solid Ga_2I_4 (0.172 g, 0.266 mmol) was dissolved in THF (4 mL). The solution turned yellow, and was allowed to stir for several hours, at which point the solvent was removed under reduced pressure. Toluene (4 mL) was added to the reaction flask, along with THF (1 drop), followed by a solution of Me_3SiOTf (0.472 g, 2.12 mmol) dissolved in toluene (2 mL). The mixture was allowed to stir for 1 h, at which point a solution of cryptand[2.2.2] (0.100 g, 0.266 mmol) dissolved in toluene (2 mL) was added, leading to the immediate formation of a white precipitate. The mixture was allowed to stir for 36 h, after which a green-grey oil had separated in the vessel. The supernatant was decanted, and the oil was triturated in CH_3CN (3 mL). A grey solid was removed by filtration, and the filtrate was dried under reduced pressure. The resultant solid was dissolved in CH_3CN (3 mL), and ether (2 mL) was added. The solution was concentrated under reduced pressure, resulting in the formation of a white precipitate. The mixture was cooled to $-20\text{ }^\circ\text{C}$ for several hours, the supernatant was decanted and the precipitate was washed with ether ($3 \times 2\text{ mL}$) and dried under reduced pressure.

Yield: 0.094 g (33%); mp: 265–268 $^\circ\text{C}$ (decomposition); ^1H NMR (600 MHz, CD_3CN , 298 K) † δ : 4.41–4.38 (m, 2H, $[\text{O}-\text{CHH}-\text{CH}_2-\text{O}]_{\text{coord}}$), 4.20–4.12 (m, 8H, $[\text{O}-\text{CHH}-\text{CH}_2-\text{N}]_{\text{coord}}$, $[\text{O}-\text{CH}_2-\text{CHH}-\text{O}]_{\text{coord}}$, $[\text{O}-\text{CH}_2-\text{CH}_2-\text{O}]_{\text{free}}$), 4.05–3.97 (m, 6H, $[\text{O}-\text{CHH}-\text{CH}_2-\text{N}]_{\text{coord}}$, $[\text{O}-\text{CHH}-\text{CH}_2-\text{N}]_{\text{free}}$), 3.92 (dddd, $J = 2\text{ Hz}, 5\text{ Hz}, 13\text{ Hz}, 19\text{ Hz}$, 2H, $[\text{O}-\text{CH}_2-\text{CHH}-\text{N}]_{\text{coord}}$), 3.86–3.76 (m, 8H, $[\text{O}-\text{CH}_2-\text{CHH}-\text{N}]_{\text{coord}}$, $[\text{O}-\text{CHH}-\text{CH}_2-\text{N}]_{\text{coord}}$, $[\text{O}-\text{CH}_2-\text{CHH}-\text{O}]_{\text{coord}}$, $[\text{O}-\text{CHH}-\text{CH}_2-\text{O}]_{\text{coord}}$), 3.73 (ddd, $J = 1\text{ Hz}, 5\text{ Hz}, 12\text{ Hz}$, 2H, $[\text{O}-\text{CHH}-\text{CH}_2-\text{N}]_{\text{coord}}$), 3.45 (ddd, $J = 1\text{ Hz}, 4\text{ Hz}, 14\text{ Hz}$, 2H, $[\text{O}-\text{CH}_2-\text{CHH}-\text{N}]_{\text{free}}$), 3.35 (dddd, $J = 1\text{ Hz}, 2\text{ Hz}, 12\text{ Hz}, 14\text{ Hz}$, 2H, $[\text{O}-\text{CH}_2-\text{CHH}-\text{N}]_{\text{free}}$), 3.19–3.16 (m, 2H, $[\text{O}-\text{CH}_2-\text{CHH}-\text{N}]_{\text{coord}}$), 3.06 (ddd, $J = 1\text{ Hz}, 2\text{ Hz}, 14\text{ Hz}$, 2H, $[\text{O}-\text{CH}_2-\text{CHH}-\text{N}]_{\text{coord}}$); $^{13}\text{C}\{^1\text{H}\}$ NMR (151 MHz, CD_3CN , 298 K) δ : 121.1 (q, $J = 321\text{ Hz}$, $[\text{O}_3\text{SCF}_3]^-$), ^{71}Ga NMR (183 MHz, CD_3CN , 298 K) δ : 121.1 (q, $J = 321\text{ Hz}$, $[\text{O}_3\text{SCF}_3]^-$), 74.47 ($[\text{O}-\text{CH}_2-\text{CH}_2-\text{O}]_{\text{free}}$), 72.26 ($[\text{O}-\text{CH}_2-\text{CH}_2-\text{O}]_{\text{coord}}$), 70.91 ($[\text{O}-\text{CH}_2-\text{CH}_2-\text{N}]_{\text{free}}$), 68.06 ($[\text{O}-\text{CH}_2-\text{CH}_2-\text{O}]_{\text{coord}}$), 66.50 ($[\text{O}-\text{CH}_2-\text{CH}_2-\text{N}]_{\text{coord}}$), 66.43 ($[\text{O}-\text{CH}_2-\text{CH}_2-\text{N}]_{\text{coord}}$), 61.14 ($[\text{O}-\text{CH}_2-\text{CH}_2-\text{N}]_{\text{coord}}$), 56.34 ($[\text{O}-\text{CH}_2-\text{CH}_2-\text{N}]_{\text{coord}}$), 55.32 ($[\text{O}-\text{CH}_2-\text{CH}_2-\text{N}]_{\text{free}}$); ^{19}F NMR (564 MHz, CD_3CN , 298 K) δ : -79.3 ($[\text{O}_3\text{SCF}_3]^-$); $^{71}\text{Ga}\{^1\text{H}\}$ NMR (183 MHz, CD_3CN , 298 K) δ : -455.4 ($[\text{GaI}_4]^-$); LR ESI-TOF MS (m/z ; positive ions): 895 ($[[^{69}\text{Ga}_2\text{I}_2(\text{crypt-222})][\text{I}]^+]$); 917 ($[[^{69}\text{Ga}_2\text{I}_2(\text{crypt-222})][\text{OTf}]^+]$); LR ESI-TOF MS (m/z ; negative ions): 149 ($[\text{OTf}]^-$); 577 ($[[^{69}\text{GaI}_4]^-]$);

HR ESI-TOF MS (m/z ; positive ions): Calcd for $\text{C}_{19}\text{H}_{36}\text{F}_3\text{I}_2\text{N}_2\text{O}_9\text{S}^{69}\text{Ga}_2$ ($[[^{69}\text{Ga}_2\text{I}_2(\text{crypt-222})][\text{OTf}]^+]$): 916.8695, Found: 916.8707; Elemental analysis (%) calcd for $[\text{Ga}_2\text{I}_2(\text{crypt-222})][\text{GaI}_4]_{1.75}[\text{OTf}]_{0.25}$ ($\text{C}_{18.25}\text{H}_{36}\text{F}_{0.75}\text{Ga}_{3.75}\text{I}_9\text{N}_2\text{O}_{6.75}\text{S}_{0.25}$): C, 12.06; H, 2.00; N, 1.54; S, 0.44; found C, 12.08; H, 2.04; N, 1.51; S, 0.39.

Synthesis of $[\text{Ga}(\text{prismand})][\text{OTf}]$, 6. $[\text{Ga}(\text{prismand})][\text{GaCl}_4]$ was synthesized according to literature procedures. 72 $[\text{Ga}(\text{prismand})][\text{GaCl}_4]$ (0.100 g, 0.142 mmol) was suspended in acetonitrile (3 mL), to which a solution of Me_3SiOTf (0.063 g, 0.284 mmol) in acetonitrile (2 mL) was added. After several hours the suspension had changed color from off-white to grey. After stirring for 36 h, the suspension was filtered, removing a grey metallic-like precipitate. The resultant solution was dried under reduced pressure, yielding an off-white residue. $^{71}\text{Ga}\{^1\text{H}\}$ NMR spectroscopy revealed that the characteristic signal for $[\text{GaCl}_4]^-$ ($\delta \sim 251\text{ ppm}$) was not present, indicating that the anion had been removed. ^{19}F NMR spectroscopy revealed the presence of the $[\text{OTf}]^-$ anion.

XPS analysis

XPS analyses were carried out with a Kratos AXIS Ultra spectrometer using a monochromatic Al $K\alpha$ (15 mA, 14 kV) X-ray source. The instrument work function was calibrated to give an Au $4f_{7/2}$ metallic gold binding energy of 83.95 eV. The spectrometer dispersion was adjusted to give a binding energy of 932.63 eV for metallic Cu $2p_{3/2}$. The Kratos charge neutralizer system was used for analyses of non-conductive samples. Charge neutralization was deemed to have been fully achieved by monitoring the C 1s signal for adventitious carbon. A sharp main peak with no lower binding energy structure is generally expected. Instrument base pressure was 9×10^{-10} Torr. Survey scans were obtained using an analysis area of $\sim 300 \times 700\ \mu\text{m}$ and a 160 eV pass energy. High resolution spectra were obtained using an analysis area of $\sim 300 \times 700\ \mu\text{m}$ and a 20 eV pass energy. A 20 eV pass energy corresponded to Ag $3d_{5/2}$ FWHM of 0.55 eV.

A single peak (Gaussian 70%–Lorentzian 30%), ascribed to alkyl type carbon (C–C, C–H), was fitted to the main peak of the C 1s spectrum for adventitious carbon. A second peak is usually added that is constrained to be 1.5 eV above the main peak, and of equal full width half maximum (FWHM) to the main peak. This higher binding energy peak is ascribed to an alcohol (C–OH) and/or ester (C–O–C) functionality. Further high binding energy components (e.g. C=O, 2.8–3.0 eV above the main peak; O–C=O, 3.6–4.3 eV above the main peak; CO_3^{2-} , 3.8–4.8 eV above the main peak) can also be added if required. Spectra from insulating samples have been charge corrected to give the adventitious C 1s spectral component (C–C, C–H) a binding energy of 284.8 eV. This process has an associated error of $\pm 0.1\text{--}0.2\text{ eV}$. 73

Survey scan analyses for selected samples are presented in the ESI.†

Spectra were analyzed using CasaXPS software (version 2.3.14). 74 Gaussian (100–X%)–Lorentzian (X%), defined in CasaXPS as GL(X), profiles were used for each component. All C 1s component species spectra have been fit with line-shapes

of GL(30). A Ga $3d_{5/2}$ –Ga $3d_{3/2}$ splitting of 0.449 eV was used for all samples. A standard Shirley background is used for all spectra.

All samples were mounted on non-conductive double sided 3M Scotch® adhesive tape. The powder samples were not sputter cleaned prior to analysis, as it is well known that this can cause reduction of oxidized species. The main stage was precooled to -130 °C prior to introducing the sample. After addition of the sample holder to the stage it was allowed to cool fully before analysis began. Cooling of the sample has been shown to reduce X-ray and thermal degradation effects in metal compounds such as copper and vanadium.⁷⁵

Acknowledgements

We thank NSERC (Canada) and University of Western Ontario for financial support. We also thank Doug Hairsine for acquiring ESI-MS data, Mathew Willans for assistance in acquiring ^{71}Ga NMR spectra

References

- In this manuscript, we distinguish between oxidation numbers, assigned using the standard formalism, and chemical states, the experimentally determined physical state of an atom in a complex. We do not use the term oxidation state to avoid ambiguity.
- G. Parkin, *J. Chem. Educ.*, 2006, **83**, 791.
- P. Atkins, *Shriver and Atkins' Inorganic Chemistry*, Oxford University Press, Oxford, England, 2010.
- C. Pubill-Ulldemolins, E. Fernandez, C. Bo and J. M. Brown, *Org. Biomol. Chem.*, 2015, **13**, 9619.
- M. Santelli and J. M. Pons, *Lewis Acids and Selectivity in Organic Synthesis*, Taylor & Francis, Boca Raton, Florida, 1995.
- A. Bonet, H. Gulyas and E. Fernandez, *Angew. Chem., Int. Ed.*, 2010, **49**, 5130.
- N. J. Hardman, R. J. Wright, A. D. Phillips and P. P. Power, *J. Am. Chem. Soc.*, 2003, **125**, 2667.
- M. J. Fink, M. J. Michalczyk, K. J. Haller, R. West and J. Michl, *J. Chem. Soc., Chem. Commun.*, 1983, 1010.
- Z. Zhu, X. Wang, M. M. Olmstead and P. P. Power, *Angew. Chem., Int. Ed.*, 2009, **48**, 2027.
- Z. Zhu, X. Wang, Y. Peng, H. Lei, J. C. Fettinger, E. Rivard and P. P. Power, *Angew. Chem., Int. Ed.*, 2009, **48**, 2031.
- B. J. Malbrecht, J. W. Dube, M. J. Willans and P. J. Ragogna, *Inorg. Chem.*, 2014, **53**, 9644.
- G. Garton and H. M. Powell, *J. Inorg. Nucl. Chem.*, 1957, **4**, 84.
- E. S. Schmidt, A. Schier, N. W. Mitzel and H. Schmidbaur, *Z. Naturforsch., B: Chem. Sci.*, 2001, **56b**, 337.
- R. P. Chapman and D. L. Bryce, *Phys. Chem. Chem. Phys.*, 2009, **11**, 6987.
- H. Schmidbaur, *Angew. Chem., Int. Ed. Engl.*, 1985, **24**, 893.
- D. Dange, S. L. Choong, C. Schenk, A. Stasch and C. Jones, *Dalton Trans.*, 2012, **41**, 9304.
- J. L. Bourque, P. D. Boyle and K. M. Baines, *Chem. – Eur. J.*, 2015, **21**, 9790.
- T. C. Gibb, *Principles of Mössbauer Spectroscopy*, Chapman and Hall, Norwich, England, 1976.
- D. P. E. Dickson and F. J. Berry, *Mössbauer Spectroscopy*, Cambridge University Press, Cambridge, England, 1986.
- S. M. Al-Rafia, O. Shynkaruk, S. M. McDonald, S. K. Liew, M. J. Ferguson, R. McDonald, R. H. Herber and E. Rivard, *Inorg. Chem.*, 2013, **52**, 5581.
- J. Henning, H. Schubert, K. Eichele, F. Winter, R. Pottgen, H. A. Mayer and L. Wesemann, *Inorg. Chem.*, 2012, **51**, 5787.
- A. M. Tondreau, C. C. H. Atienza, J. M. Darmon, C. Milsmann, H. M. Hoyt, K. J. Weller, S. A. Nye, K. M. Lewis, J. Boyer, J. G. P. Delis, E. Lobkovsky and P. J. Chirik, *Organometallics*, 2012, **31**, 4886.
- M. A. Hanson, V. V. Terskikh, K. M. Baines and Y. Huang, *Inorg. Chem.*, 2014, **53**, 7377.
- C. Engemann, R. Franke, J. Hormes, C. Lauterbach, E. Hartmann, J. Clade and M. Jansen, *Chem. Phys.*, 1999, **243**, 61.
- A. N. Mansour, C. A. Melendres, M. Pankuch and R. A. Brizzolara, *J. Electrochem. Soc.*, 1994, **141**, L69.
- Y. N. Vodyanitskii, *Eurasian Soil Sci.*, 2014, **46**, 1139.
- M. J. Ward, P. A. Rugar, M. W. Murphy, Y. M. Yiu, K. M. Baines and T. K. Sham, *Chem. Commun.*, 2010, **46**, 7016.
- P. van der Heide, *X-ray Photoelectron Spectroscopy: An Introduction to Principles and Practices*, John Wiley & Sons, Inc., Hoboken, New Jersey, 2012.
- C. D. Wagner, *Anal. Chem.*, 1972, **44**, 967.
- G. Moretti, *J. Electron Spectrosc. Relat. Phenom.*, 1998, **95**, 95.
- M. C. Biesinger, L. W. Lau, A. R. Gerson and R. S. Smart, *Phys. Chem. Chem. Phys.*, 2012, **14**, 2434.
- C. D. Wagner and A. Joshi, *J. Electron Spectrosc. Relat. Phenom.*, 1988, **47**, 283.
- G. Moretti, *Surf. Sci.*, 2013, **618**, 3.
- J. F. Watts and J. Wolstenholme, *An Introduction to Surface Analysis by XPS and AES*, Wiley, Chichester, England, 2003.
- G. E. McGuire, G. K. Schweitzer and T. A. Carlson, *Inorg. Chem.*, 1973, **12**, 2450.
- Y. Mizokawa, H. Iwasaki, R. Nishitani and S. Nakamura, *J. Electron Spectrosc. Relat. Phenom.*, 1978, **14**, 129.
- R. Nishitani, H. Iwasaki, Y. Mizokawa and S. Nakamura, *Jpn. J. Appl. Phys.*, 1978, **17**, 321.
- J. Hedman and N. Mårtensson, *Phys. Scr.*, 1980, **22**, 176.
- H. Iwakuro, C. Tatsuyama and S. Ichimura, *Jpn. J. Appl. Phys.*, 1982, **21**, 94.
- F. Stepniak, D. Rioux and J. Weaver, *Phys. Rev. B: Condens. Matter*, 1994, **50**, 1929.
- W. C. Simpson, D. K. Shuh, W. H. Hung, M. C. Hakansson, J. Kanski, U. O. Karlsson and J. A. Yarmoff, *J. Vac. Sci. Technol., A*, 1996, **14**, 1815.

- 42 W.-H. Hung, S.-L. Wu and C.-C. Chang, *J. Phys. Chem. B*, 1998, **102**, 1141.
- 43 A. Shaporenko, K. Adlkofer, L. S. O. Johansson, A. Ulman, M. Grunze, M. Tanaka and M. Zharnikov, *J. Phys. Chem. B*, 2004, **108**, 17964.
- 44 T. Mayer, M. V. Lebedev, R. Hunger and W. Jaegermann, *J. Phys. Chem. B*, 2006, **110**, 2293.
- 45 C. D. Wagner, D. E. Passoja, H. F. Hillery, T. G. Kinisky, H. A. Six, W. T. Jansen and J. A. Taylor, *J. Vac. Sci. Technol.*, 1982, **21**, 933.
- 46 R. Reiche, D. Dobler, J. P. Holgado, A. Barranco, A. I. Martín-Concepción, F. Yubero, J. P. Espinós and A. R. González-Elipe, *Surf. Sci.*, 2003, **537**, 228.
- 47 G. Schön, *J. Electron Spectrosc. Relat. Phenom.*, 1973, **2**, 75.
- 48 C. D. Wagner, *Faraday Discuss. Chem. Soc.*, 1975, **60**, 291.
- 49 S. Evans, *Surf. Interface Anal.*, 1985, **7**, 299.
- 50 C. D. Wagner and G. E. Muilenberg, *Handbook of X-ray photoelectron spectroscopy: a reference book of standard data for use in X-ray photoelectron spectroscopy*, Physical Electronics Division, Perkin-Elmer Corp., 1979.
- 51 Y. Mizokawa, H. Iwasaki and S. Nakamura, *Jpn. J. Appl. Phys.*, 1981, **20**, L491.
- 52 A. Y. Timoshkin, M. Bodensteiner, T. N. Sevastianova, A. S. Lisovenko, E. I. Davydova, M. Scheer, C. Grassl and A. V. Butlak, *Inorg. Chem.*, 2012, **51**, 11602.
- 53 S. C. Wallwork and I. J. Worrall, *J. Chem. Soc.*, 1965, 1816.
- 54 N. J. Hardman, B. E. Eichler and P. P. Power, *Chem. Commun.*, 2000, 1991.
- 55 J. C. Beamish, R. W. H. Small and I. J. Worrall, *Inorg. Chem.*, 1979, **18**, 220.
- 56 O. T. Beachley, M. R. Churchill, J. C. Pazik and J. W. Ziller, *Organometallics*, 1987, **6**, 2088.
- 57 M. B. Smith, *Organic Chemistry: An Acid–Base Approach*, CRC Press, Boca Raton, Florida, 2010.
- 58 N. J. Hardman, P. P. Power, J. D. Gorden, C. L. B. Macdonald and A. H. Cowley, *Chem. Commun.*, 2001, 1866.
- 59 S. P. Green, C. Jones, K. A. Lippert, D. P. Mills and A. Stasch, *Inorg. Chem.*, 2006, **45**, 7242.
- 60 O. T. Beachley, J. R. Gardinier and M. R. Churchill, *Organometallics*, 2000, **19**, 4544.
- 61 C. E. Housecroft and A. G. Sharpe, *Inorganic Chemistry*, Pearson Prentice Hall, Harlow, England, 2008.
- 62 S. S. Kumar, E. J. Rubio, M. Noor-A-Alam, G. Martinez, S. Manandhar, V. Shutthanandan, S. Thevuthasan and C. V. Ramana, *J. Phys. Chem. C*, 2013, **117**, 4194.
- 63 M. L. H. Green, P. Mountford, G. J. Smout and S. R. Speel, *Polyhedron*, 1990, **9**, 2763.
- 64 R. J. Baker, R. D. Farley, C. Jones, M. Kloth and D. M. Murphy, *J. Chem. Soc., Dalton Trans.*, 2002, 3844.
- 65 R. J. Baker, H. Bettentrup and C. Jones, *Eur. J. Inorg. Chem.*, 2003, **2003**, 2446.
- 66 O. Serrano, J. C. Fettinger and P. P. Power, *Polyhedron*, 2013, **58**, 144.
- 67 T. Yamaguchi, K. Ueno and H. Ogino, *Organometallics*, 2001, **20**, 501.
- 68 J. C. Beamish, M. Wilkinson and I. J. Worrall, *Inorg. Chem.*, 1978, **17**, 2026.
- 69 E. S. Schmidt, A. Schier and H. Schmidbaur, *J. Chem. Soc., Dalton Trans.*, 2001, 505.
- 70 The subscript “coord” refers to the two arms of cryptand [2.2.2] coordinated to the gallium centers; the subscript “free” refers to the arm of cryptand[2.2.2] that is not coordinated to a gallium center.
- 71 The chemical shift of the carbon atom in the triflate anion was obtained using a $^{13}\text{C}\{^1\text{H}\}-^{19}\text{F}$ HSQC experiment.
- 72 A. Kunze, R. Gleiter, S. Bethke and F. Rominger, *Organometallics*, 2006, **25**, 4787.
- 73 D. J. Miller, M. C. Biesinger and N. S. McIntyre, *Surf. Interface Anal.*, 2002, **33**, 299.
- 74 N. Fairley, *Casa XPS*, Casa Software Ltd, 2005.
- 75 M. C. Biesinger, L. W. M. Lau, A. R. Gerson and R. S. C. Smart, *Appl. Surf. Sci.*, 2010, **257**, 887.

Supplementary Information: Bourque *et al.*

Supplementary Information for:

Chemical State Determination of Molecular Gallium Compounds using XPS

Jeremy L. Bourque,¹ Mark C. Biesinger² and Kim M. Baines*¹

¹ Department of Chemistry, University of Western Ontario, London, Ontario, Canada N6A 5B7

² Surface Science Western, University of Western Ontario, London, Ontario, Canada, N6G 0J3

Table S1	S2
Figure S1	S4
Figure S2	S5
Figure S3	S6
Figure S4	S7
Figure S5	S8
Table S2	S9

Table S1: Tabulated survey scans for compounds 1 - 15, 19.

Compound	Atomic Percentage (%)													
	C	N	O	F	Na	Mg	Si	S	Cl	K	Ca	Ga	Br	I
1	56.5	-	19.1	0.3	-	-	-	-	14.3	-	-	9.5	-	0.4
2	50.3	-	21.7	7.2	-	-	-	-	12.1	-	-	8.6	-	-
3	57.1	-	23.9	9.6	-	-	-	2.6	-	-	-	2.3	-	4.5
4	90.3	3.5	2.2	-	-	-	-	-	0.3	-	-	3.1	-	0.6
5	65.5	-	18.1	1.3	-	-	0.3	-	2.7	8.9	-	2.2	-	0.9
6	50.3	-	25.0	15.8	-	-	1.8	5.0	-	-	-	2.0	-	0.1
7	51.7	-	19.0	-	-	-	-	-	19.9	-	-	9.5	-	-
8	68.7	-	15.1	-	-	-	-	-	-	-	-	6.5	-	9.7
9	85.1	-	8.3	-	-	-	-	-	-	-	-	3.5	-	3.1
10	41.9	-	17.0	5.6	0.4	-	-	-	21.8	-	-	13.4	-	-
11	67.5	-	10.0	1.4	0.2	-	-	-	-	-	-	6.9	12.6	1.3
12	53.4	-	10.2	-	-	-	-	-	-	-	-	8.2	-	28.3
13	42.6	-	20.3	3.6	-	0.6	-	-	19.7	-	0.6	12.2	-	0.3
14	34.9	-	10.0	42.4	-	-	-	-	7.8	-	-	4.9	-	-
15	55.1	-	16.0	18.3	-	-	-	-	-	-	-	4.2	-	6.4
19	8.7	-	55.5	-	-	-	-	-	0.2	-	-	35.5	-	-

Note: Varying levels of contamination were observed for most of the samples analyzed.

Common contaminants were found to be iodine, oxygen, carbon, and fluorine. The source of the iodine is postulated to come from cross-contamination arising from the vacuum chamber of the XPS instrument, as it was not only observed in samples related to this study, but in other data

from unrelated work. Carbon and oxygen arise from the adhesive tape used in sample preparation. Alternatively, the oxygen could have been a result of possible oxidation of the samples. Despite the use of an argon filled glovebox for sample preparation and introduction to the XPS instrument, the sensitivity of the gallium compounds to oxygen and water could have lead to some oxidation on the surface of some samples, causing oxygen contamination, however, because of the strict anaerobic conditions employed, this was assumed to be negligible. Any additional carbon and oxygen contamination could be resulting from excess solvent present in the samples, due to incomplete drying. The presence of fluorine in the survey spectra is likely a result of the fluoropolymer lining in the sample vial caps, which were used for synthesis and transportation of the samples. Overall, none of the contaminants were believed to interfere with any of the results of this study, as the gallium signals were used for characterization and assignment for all compounds, of which there was no contamination source.

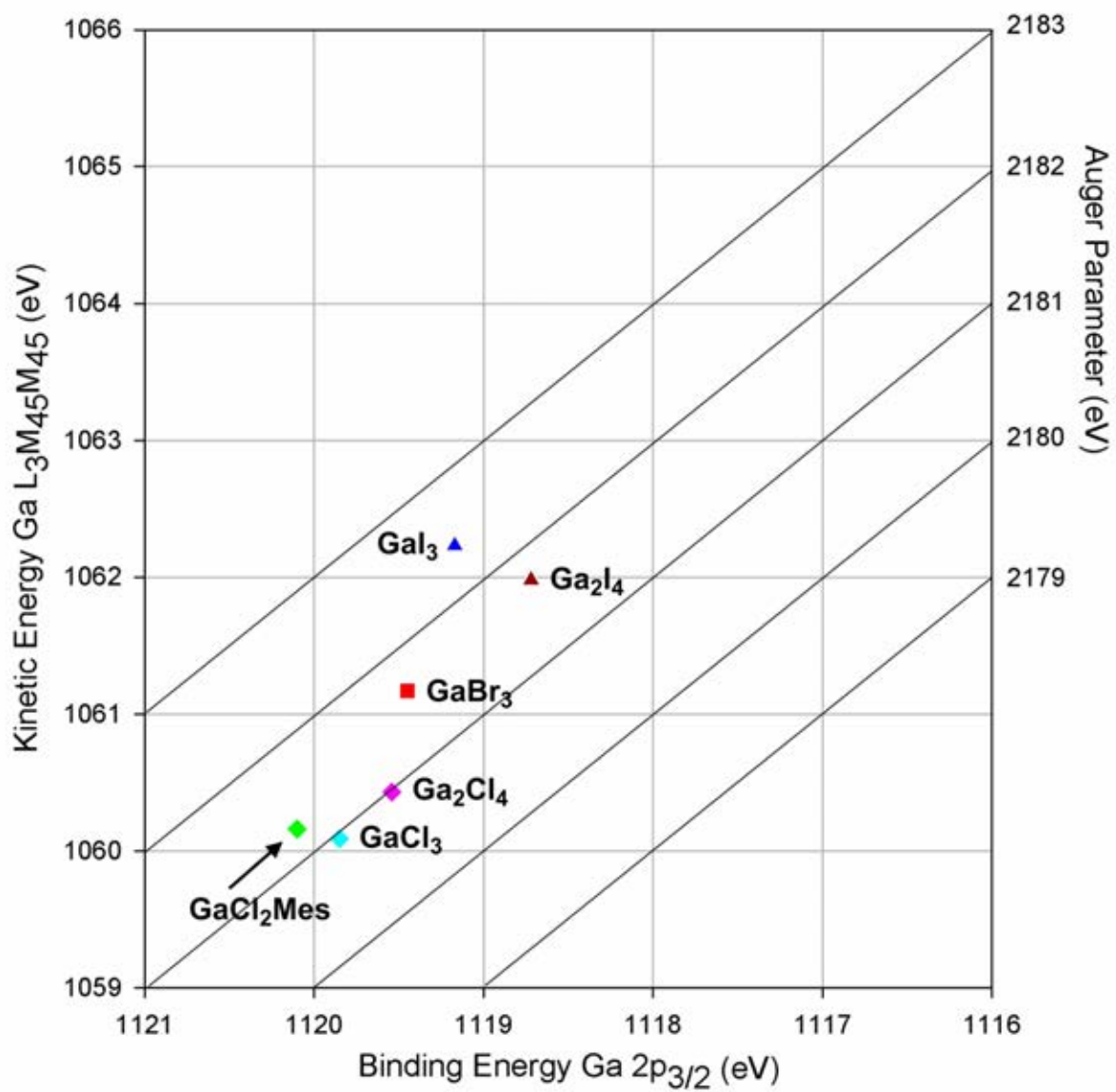


Figure S1: Wagner plot of gallium halides using Ga 2p_{3/2} binding energy. Symbol legend: diamond = chloride ligands; square = bromide ligands; triangle = iodide ligands.

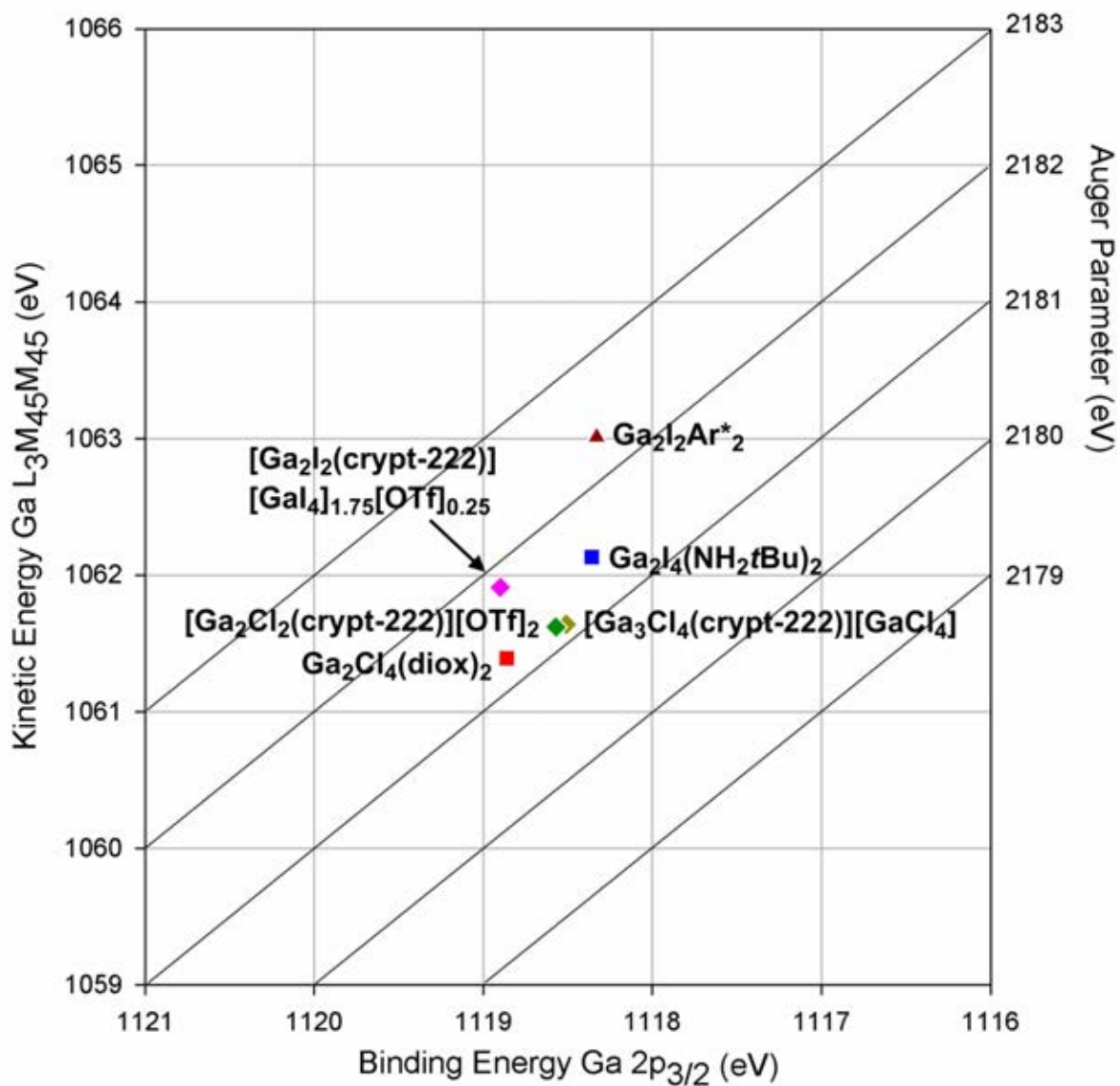


Figure S2: Wagner plot of Ga-Ga compounds using Ga 2p_{3/2} binding energy. Symbol legend: diamond = synthesized gallium-cryptand complexes; square = chloride and iodide ligands and O/N donors; triangle = iodide and terphenyl ligands.

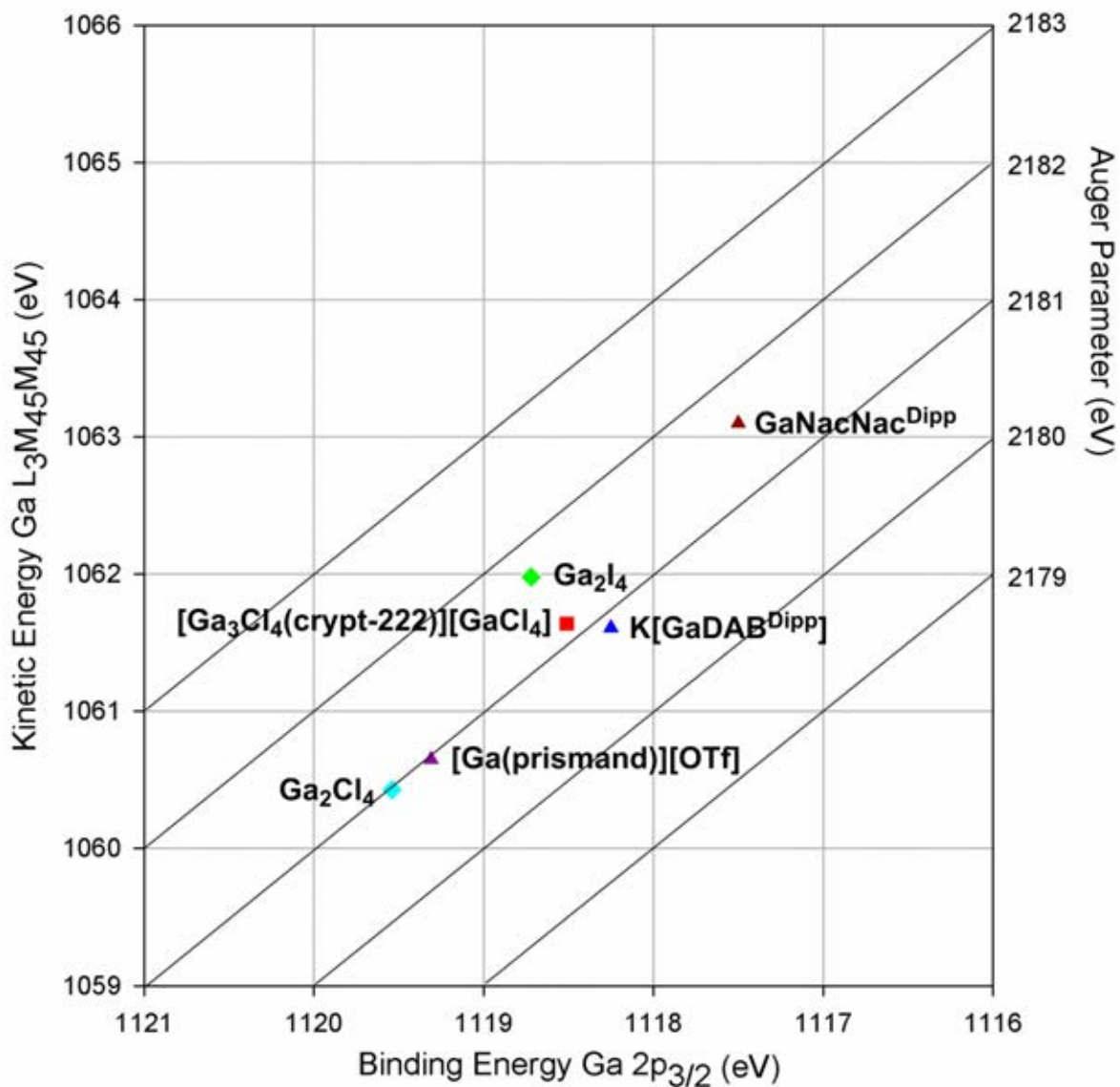


Figure S3: Wagner plot of Ga(I) compounds using Ga 2p_{3/2} binding energy. Symbol legend: diamond = halide ligands; square = chloride ligands and O/N donors; triangle = organic ligands.

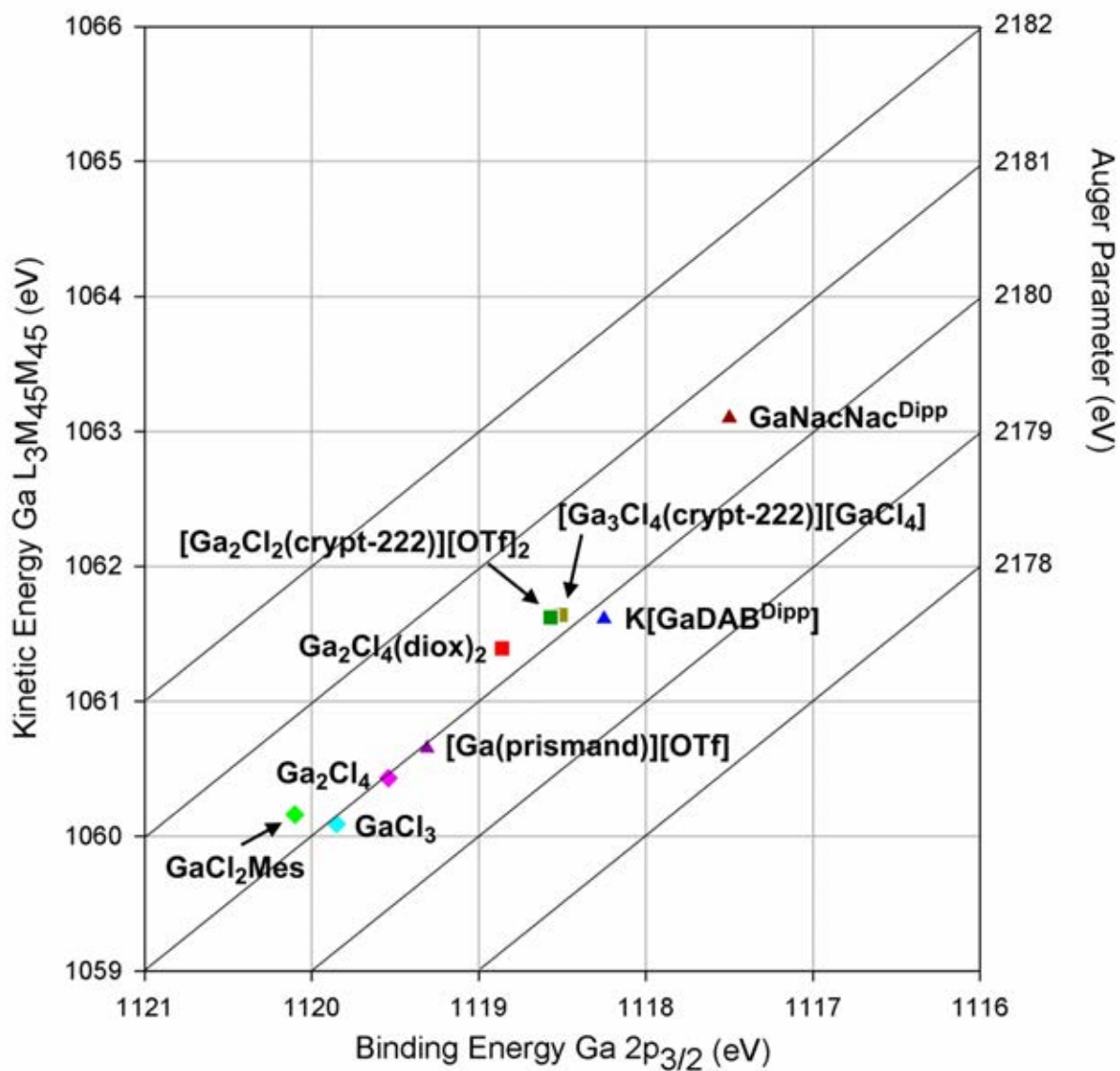


Figure S4: Wagner plot of gallium-chloride and gallium-nitrogen compounds using Ga 2p_{3/2} binding energy. Symbol legend: diamond = Ga(III); square = Ga(II); triangle = Ga(I).

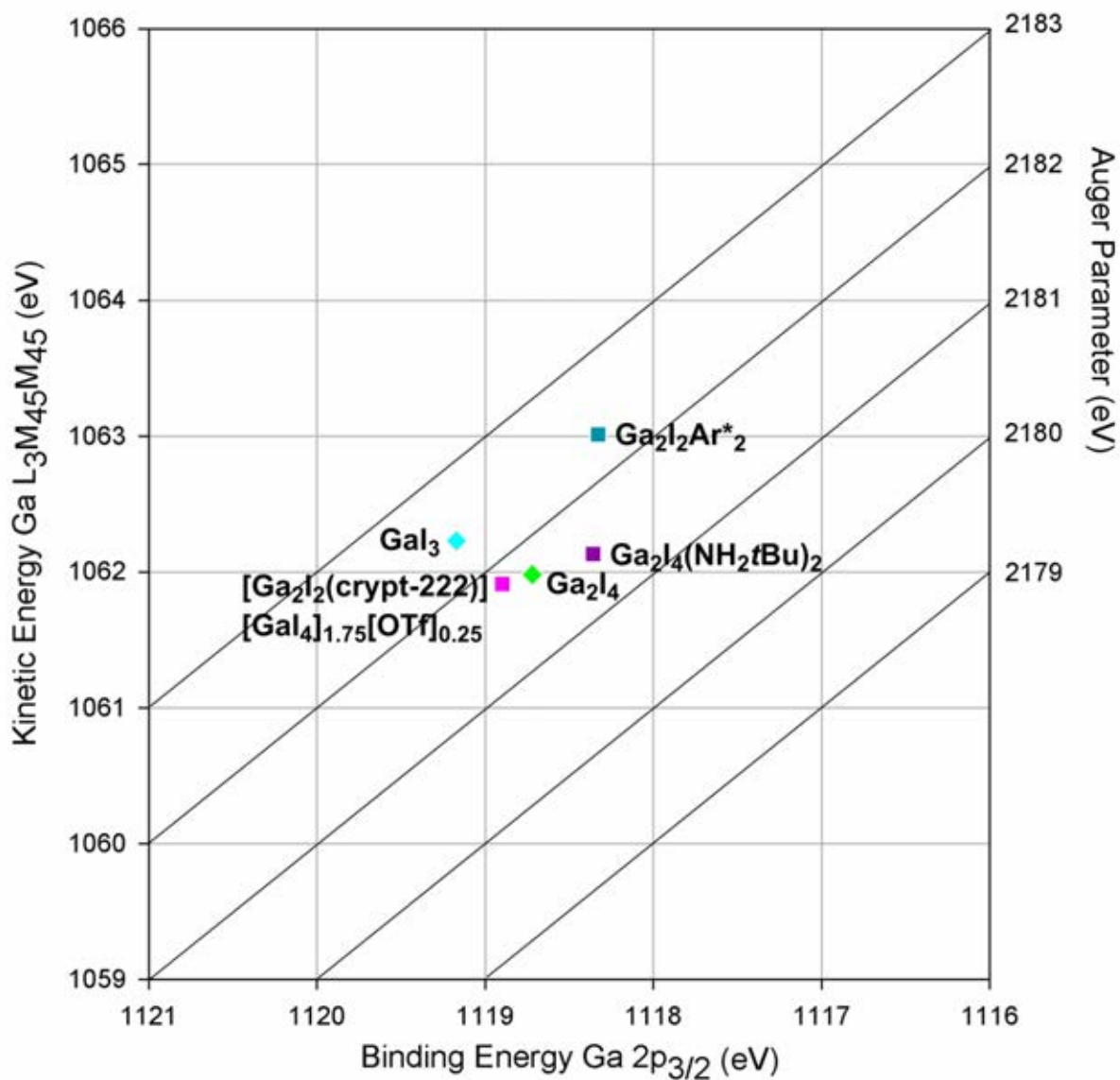


Figure S5: Wagner plot of gallium-iodide compounds using Ga 2p_{3/2} binding energy. Symbol legend: diamond = Ga(III); square = Ga(II).

Table S2: Auger parameters and relevant shifts for compounds analyzed using Ga 2p_{3/2} binding energy.

Compound	Auger Parameter, α' (eV)	ΔE_B (eV)	ΔE_K (eV)	Relaxation Shift, $\Delta\alpha'$ (eV)	Final State Shift, ΔR (eV)	Initial State Shift, $\Delta\epsilon$ (eV)
Ga_(m) (meas)	2184.50	-	-	-	-	-
Ga_(m) (lit)	2184.88	-	-	-	-	-
4	2180.60	1.01	-4.91	-3.90	-1.95	0.94
5	2180.86	1.76	-6.40	-4.64	-2.32	0.56
6	2180.96	2.82	-7.36	-3.54	-1.77	-1.05
7	2180.25	2.37	-6.62	-4.25	-2.13	-0.25
8	2180.49	1.87	-5.88	-4.01	-2.01	0.14
9	2181.34	1.84	-5.00	-3.16	-1.58	-0.26
10	2179.94	3.36	-7.92	-4.56	-2.28	-1.08
11	2180.62	2.96	-6.84	-3.88	-1.94	-1.02
12	2181.40	2.68	-5.78	-3.10	-1.55	-1.13
13	2180.26	3.61	-7.85	-4.24	-2.12	-1.49
14	2179.97	3.05	-7.58	-4.53	-2.27	-0.79
15	2180.70	2.23	-6.03	-3.80	-1.90	-0.33
18	2183.30	0.41	-1.61	-1.20	-0.60	0.19
19 (meas)	2180.40	1.31	-5.41	-4.10	-2.05	0.74
19 (lit)	2180.25	0.96	-5.16	-4.25	-2.13	1.22
1	2180.15	2.02	-6.37	-4.35	-2.18	0.16
2	2180.19	2.08	-6.39	-4.31	-2.16	0.08
3	2180.81	2.41	-6.10	-3.69	-1.85	-0.57